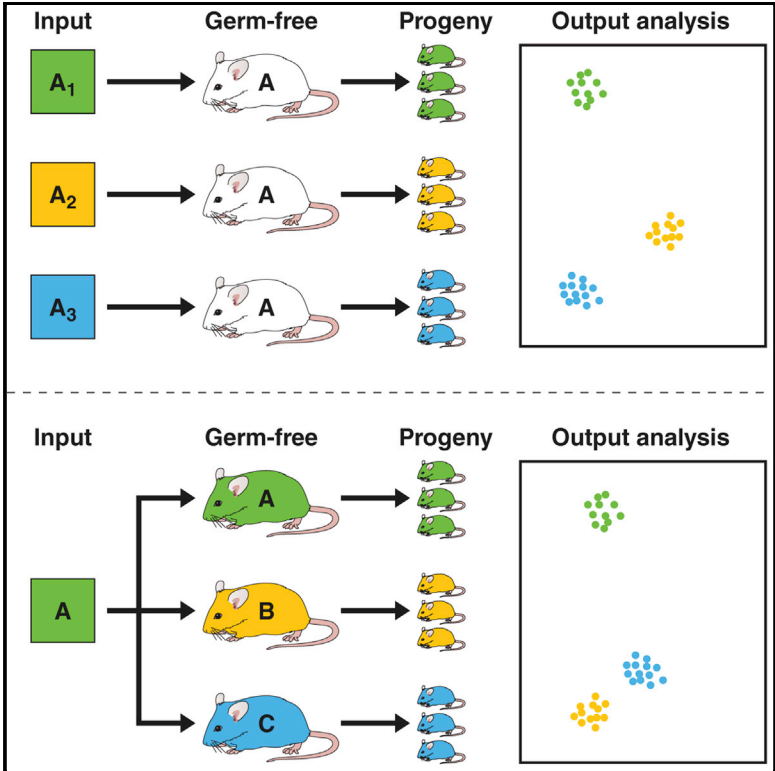


Polymorphic Immune Mechanisms Regulate Commensal Repertoire

Graphical Abstract



Authors

Aly A. Khan, Leonid Yurkovetskiy, Kelly O’Grady, ..., Dionysios A. Antonopoulos, Tatyana Golovkina, Alexander Chervonsky

Correspondence

tgolovki@bsd.uchicago.edu (T.G.), achervon@bsd.uchicago.edu (A.C.)

In Brief

The importance of polymorphic genes in shaping commensal repertoire is unclear. Khan et al. use genetically different GF mice transferred with identical microbiotas to show that polymorphism in both innate and adaptive immune mechanisms influence the output microbiomes. These mechanisms are likely to work in concert with non-polymorphic microbiota-controlling mechanisms.

Highlights

- Input microbiota defines output microbiomes upon transfer in syngeneic GF mice
- Genetic backgrounds define outputs after transfer with identical input microbiota
- Polymorphisms in innate and adaptive immunity genes affect commensal composition
- Some microbes may use immune mechanisms for their own advantage



Polymorphic Immune Mechanisms Regulate Commensal Repertoire

Aly A. Khan,^{1,2} Leonid Yurkovetskiy,^{2,3,8} Kelly O'Grady,⁴ Joseph M. Pickard,^{2,5,9} Renée de Pooter,² Dionysios A. Antonopoulos,^{6,7} Tatyana Golovkina,^{3,4,5,*} and Alexander Chervonsky^{2,3,5,10,*}

¹Toyota Technological Institute at Chicago, Chicago, IL 60637, USA

²Department of Pathology, University of Chicago, Chicago, IL 60637, USA

³Committee on Microbiology, University of Chicago, Chicago, IL 60637, USA

⁴Department of Microbiology, University of Chicago, Chicago, IL 60637, USA

⁵Committee on Immunology, University of Chicago, Chicago, IL 60637, USA

⁶Department of Medicine, University of Chicago, Chicago, IL 60637, USA

⁷Biosciences Division, Argonne National Laboratory, Lemont, IL 60439, USA

⁸Present address: Department of Molecular Medicine, University of Massachusetts Medical School, Worcester, MA, USA

⁹Present address: Department of Pathology and Rogel Cancer Center, University of Michigan Medical School,

1500 East Medical Center Drive, Ann Arbor, MI 48109, USA

¹⁰Lead Contact

*Correspondence: tgolovki@bsd.uchicago.edu (T.G.), achervon@bsd.uchicago.edu (A.C.)

<https://doi.org/10.1016/j.celrep.2019.09.010>

SUMMARY

Environmental influences (infections and diet) strongly affect a host's microbiota. However, host genetics may influence commensal communities, as suggested by the greater similarity between the microbiomes of identical twins compared to non-identical twins. Variability of human genomes and microbiomes complicates the understanding of polymorphic mechanisms regulating the commensal communities. Whereas animal studies allow genetic modifications, they are sensitive to influences known as “cage” or “legacy” effects. Here, we analyze ex-germ-free mice of various genetic backgrounds, including immunodeficient and major histocompatibility complex (MHC) congenic strains, receiving identical input microbiota. The host's polymorphic mechanisms affect the gut microbiome, and both innate (anti-microbial peptides, complement, pentraxins, and enzymes affecting microbial survival) and adaptive (MHC-dependent and MHC-independent) pathways influence the microbiota. In our experiments, polymorphic mechanisms regulate only a limited number of microbial lineages (independently of their abundance). Our comparative analyses suggest that some microbes may benefit from the specific immune responses that they elicit.

INTRODUCTION

Commensal microbes are indispensable for the existence of their eukaryotic hosts and provide essential functions (nutrition and pathogen colonization resistance) required for the host's survival, as well as performing a number of accessory functions

such as influencing the status of the immune system, vascularization, and behavior (Belkaid and Hand, 2014). The composition of microbial communities varies from individual to individual and is shaped by multiple factors, including the mode of transmission during birth, breastfeeding, alimentary infections, and diet. The overall microbial composition can change rapidly in response to the latter two factors (Carmody et al., 2015; Rothschild et al., 2018), but tends to return to the pre-challenge state (David et al., 2014), albeit with some irreversible losses (Sonnenburg et al., 2016). Previous studies suggested that the host's genetics shape the microbial repertoire. Microbiotas cross-transplanted between animals of distant classes acquire features dictated by the new host (Rawls et al., 2006), which could be an extreme example. A more proximate example is the greater similarity of the microbiomes between identical twins than between non-identical twins (Goodrich et al., 2014, 2016). However, two important questions remain unanswered: to what extent and which host's polymorphic mechanisms are involved in shaping the repertoire of the commensals?

Since genetic manipulation in humans is not possible, these issues could only be addressed by animal experiments. The animal approach has intrinsic problems that are illustrated by conflicting findings made by using the same mouse strains at different institutions (Elinav et al., 2018; Wullaert et al., 2018). These discrepancies arise because, even with other environmental factors held constant, variation in the colonizing input microbiota defines the outcomes. Several approaches can be used to reduce the influence of “cage” or “legacy” effects, such as using littermates or the single housing of animals. However, the litter size usually limits the numbers of animals of different genotypes available for statistical analyses, so that the cage effects from separate housing of animals of different genotypes inevitably confound experimental outcomes.

Here, by using the same input microbiota to colonize genetically distinct germ-free (GF) animals, we learned how polymorphic host genes shape the intestinal microbial communities.



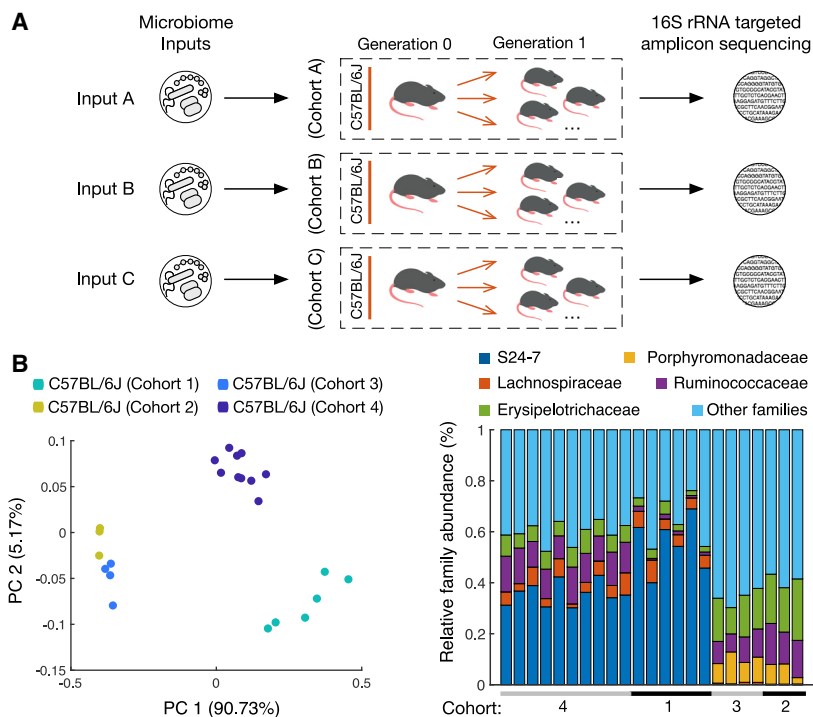


Figure 1. Input Microbiome Defines the Output Microbiota Composition in Genetically Identical Gnotobiotic Mice

(A) Experimental scheme. Generation 0 (G0) mice were transferred with cecal contents from C57BL/6J mice (input microbiota). Generation 1 (G1) progeny were used to isolate cecal microbial DNA at 8 weeks of age. DNA was analyzed by targeted amplicon sequencing of 16S rRNA encoding genes. Experiments were repeated multiple times with variable input.

(B) Principal-component analysis (PCA) of the microbiomes of ex-germ-free C57BL/6J female mice transferred with C57BL/6J microbiota in four independent experiments (left panel) and relative abundance of common taxonomic families (right panel) in the microbiomes of individual mice from the same experiments. Colored dots, individual mice. The numbers of animals from all of the cohorts used in experiments are shown in Table S1.

RESULTS

First, we sought to define to what extent the input microbiota determines the outcome of colonization experiments (Figure 1A). We performed several independent experiments colonizing GF C57BL/6J (B6) mice with the cecal contents of specific-pathogen-free (SPF) B6 mice either obtained from The Jackson Laboratory (JAX) and maintained in our colony (B6-UC, cohort 1), straight from JAX (JAX, cohort 4), or straight from Taconic (B6-TAC, cohorts 2 and 3) (Table S1). In all of the experiments, female recipient mice (G0) were colonized within minutes of obtaining donor material inside gnotobiotic isolators and were bred to produce offspring (G1). Subsequently, the microbiomes of 8-week-old G1 mice were analyzed by 16S rRNA targeted amplicon sequencing. G1 microbiomes did not segregate from the microbiomes of the G0 mothers (Figure S1). However, principal-component analysis (PCA) of the sequencing results of the female microbiomes obtained from the SPF B6 to GF B6 microbiota transfers clearly segregated recipients (cohorts 1–4) by different input (Figure 1B; Table S1) visualizing the legacy effects (Figure 1B; Table S1). Thus, finding a clear definition for a “B6-specific microbiome” was not a trivial task.

This problem, however, does not preclude comparison of the microbiomes of mice from different strains within the same microbiota transfer experiment (Figure 2A; a combined summary of strain usage for all of the experiments in this study is shown in Table S1). The transfer of SPF B6 cecal contents to GF B6, GF BALB/cJ, and GF C3H/HeN mice resulted in the clear segregation of commensal repertoires in the recipients (Figures 2B, 2C, and S2A–S2G). Previously reported gender-driven differences of microbiomes within a given strain (Yurkovetskiy et al., 2013) were

also detectable in this study (Figures 2D and S2H). These differences, however, appeared to be dominated by microbiome differences between strains (Figures 2E and S2H), allowing us to include mice of both genders in strain comparisons.

Second, we sought to test whether the abundance of specific microbes was associated with the genetic background of the host. Comparisons of the BALB/c and B6 microbiomes from 3 independent microbiota transfer experiments, in which B6-UC or B6-TAC microbiota donors were used, identified bacterial lineages with a statistically significant variation ($p < 0.05$, false discovery rate [FDR]-adjusted t test) in abundance between the two recipient mouse strains (Figures 2F–2H). Moreover, three lineages defined as *Turicibacter*, and members of the *Clostridiaceae* and *Peptostreptococcaceae* families were excluded from BALB/c microbiomes in cohorts 1 and 3 and were present in B6 microbiomes independently of the mouse gender (Figures 2F and 2G). However, in the third experiment (cohort 2; Figures 2H and S2F), these lineages were not rendered as different in the microbiomes of recipient BALB/c and B6 mice. When the relative abundances of these lineages in B6 mice were compared between all of the experiments, it became clear that two lineages (*Turicibacter* and members of family *Peptostreptococcaceae*) were undetectable and one lineage (members of family *Clostridiaceae*) was reduced in the B6 mice from cohort 2 compared to the B6 mice from other cohorts (Figure 2I). Thus, this result could be simply explained by the paucity of these lineages in the microbiota of the donor used in this experiment.

Figures 2J and 2K (and Figures S2C and S2D) illustrate the establishment of distinct microbiome patterns between another two unrelated mouse strains, BALB/cJ and C3H/HeN (cohort 1), that we transferred with the same input microbiota.

The microbiomes are likely shaped by different forces, including immune (innate and adaptive) mechanisms, which differ in the ways that they sense the microbiota and in the effector

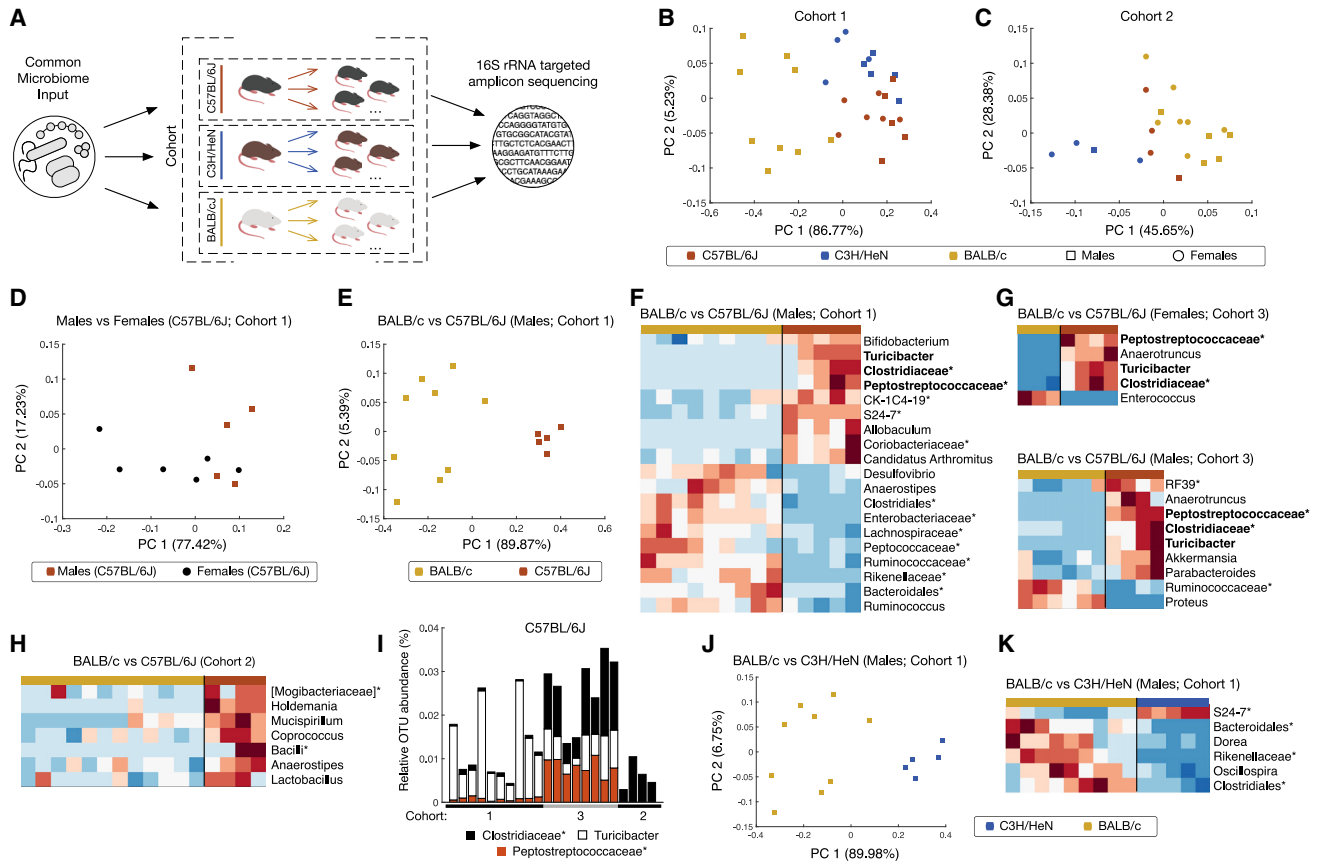


Figure 2. Mouse Strains Shape Intestinal Microbiota Composition in a Genetic Background- and an Input-Dependent Manner

(A) Experimental scheme. Within the same cohort, GF mice of different genetic backgrounds were repopulated with cecal microbiota from the same input source. The cecal microbiota of their progeny was obtained at 8 weeks of age and analyzed by sequencing 16S rRNA gene amplicons.

(B and C) Microbiomes of mice from three ex-GF mouse strains (C57BL/6J [red], C3H/HeN [blue], and BALB/cJ [orange]) repopulated with the microbiota from SPF C57BL/6 mice in two independent experiments (cohorts 1, B, and 2, C) were compared by PCA analysis using a relative abundance of bacterial genera. Individual mice are represented by rectangles (males) and circles (females).

(D) Comparison of the microbiomes of ex-GF C57BL/6J males and females from cohort 1. Males are represented by red rectangles and females by black circles.

(E–H) Comparison of the microbiomes of two ex-GF strains (C57BL/6J and BALB/cJ) colonized with the same microbiotas shown as PCA (E), or as heatmaps for lineages with statistically significant differences ($p < 0.05$, FDR-adjusted t test) in cohorts 1 (F), 3 (G), and (H). Non-specific genera identified at family, order, or class level are marked with an asterisk. Lineages that are commonly present in mice of the same genetic background in more than one experiment are in bold.

(I) Relative operational taxonomic unit (OTU) abundance of the 3 lineages that were found enhanced in C57BL/6J mice compared to BALB/cJ mice in cohorts 1 and 3, but not in cohort 2 (see Figure S2).

(J and K) Comparison of the microbiomes of ex-GF BALB/cJ and C3H/HeN mice repopulated with the same microbiota from a C57BL/6J donor (J) and heatmaps for statistically significant lineage differences ($p < 0.05$, FDR-adjusted t test) (K).

mechanisms triggered by the recognition. Adaptive mechanisms based on T cell reactivity and/or T cell-dependent antibody responses rely on antigen presentation by molecules of the major histocompatibility complexes (MHCs) expressed on the surface of specialized cells. To address the importance of MHCs in shaping the microbiomes, we rederived four additional GF strains—BALB/c.H-2ⁱ (congenic to BALB/c with the H-2ⁱ MHC allele derived from I/LnJ mice; Figure S3A); BALB.B (congenic to BALB/c, but carrying the MHC H-2^b allele found in B6 mice); and another pair of strains, I/LnJ (H-2^j) and I/LnJ.H-2^k (congenic to I/LnJ, carrying the H-2^k MHC allele from C3H/He mice; Figure S3A)—and used them as recipients in microbiota transfer experiments. In one of the experiments, the microbiomes of ex-GF BALB/cJ mice (H-2^d) were compared to the microbiomes of ex-

GF BALB/c.H-2^j (H-2^j) as well as to unrelated B6 and C3H/HeN mice (Figure 3A). The distinction between the microbiomes of these two BALB-based MHC congenic strains when simultaneously compared to B6 and C3H microbiomes was visualized by a 3-dimensional PCA plot (cohort 1; Figure 3A). That distinction was not as obvious in the 2-dimensional (2D) plot (Figure S3B) due to the shorter distance between BALB/c and BALB/c-H-2^j microbiomes compared to their distance from B6 and C3H/HeN microbiomes in PCA space. A direct comparison of the two microbiomes (Figures 3B and S3C) revealed their separation. Comparison of the microbiomes of other MHC congenic mice, BALB/c (H-2^d) and BALB.B (H-2^b) (cohort 2; Figures 3C and S3D), revealed differences between them as well. The microbiomes of I/LnJ (H-2^j) and I/LnJ.C3H (H-2^k) repopulated with the B6

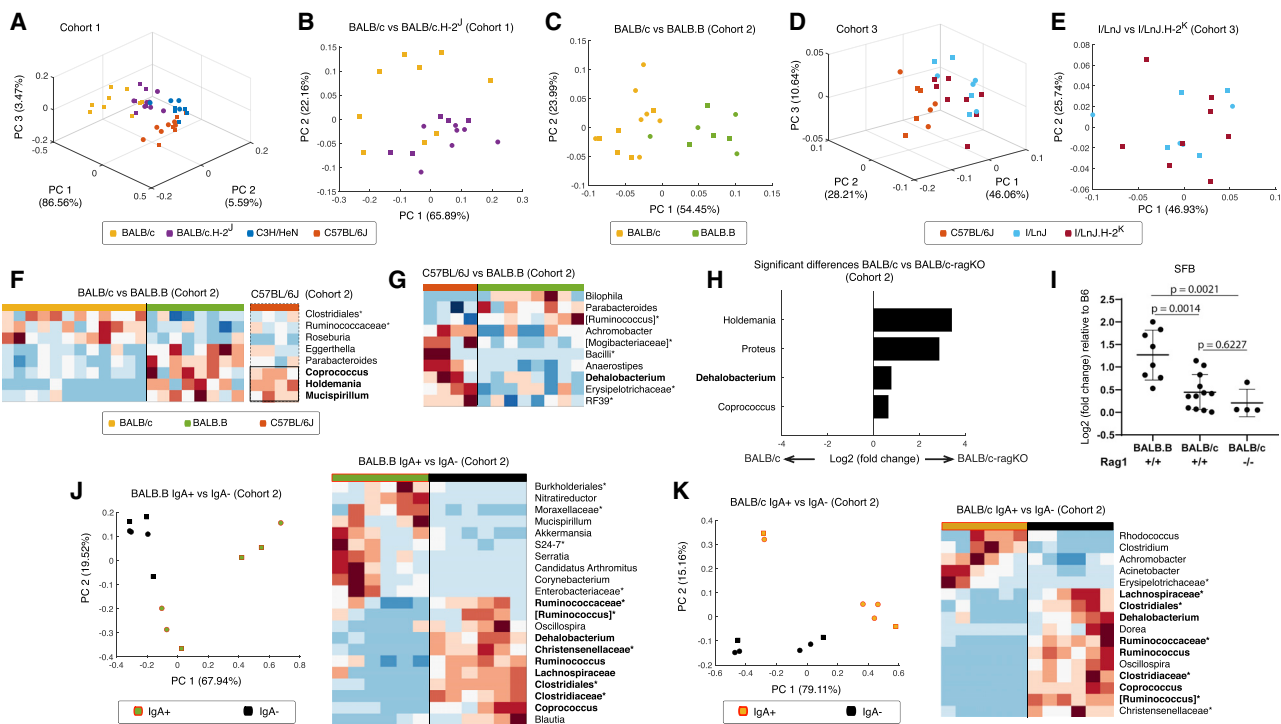


Figure 3. MHC-Dependent and -Independent Adaptive Mechanisms Contribute Moderately to the Shaping of the Intestinal Microbiota

(A) Mutual positioning of the microbiomes of MHC congenic strains BALB/cJ (H-2^d) and BALB/c (H-2^b) compared to positions of the microbiomes of C57BL/6J and C3H/HeN mice in PCA space (see also Figure S3).

(B and C) Pairwise comparisons of the microbiomes of mice from MHC congenic strains BALB/c versus BALB/c.H-2^d (B) and BALB/c versus BALB.B (C).

(D) Microbiomes of ex-GF C57BL/6J mice compared to the microbiomes of a pair of MHC congenic strains (I/LnJ [H-2] and I/LnJ.H-2^k) transferred with the same microbiota.

(E) Pairwise analysis of I/LnJ and I/LnJ.H-2^k microbiomes from the same experiment.

(F) Statistically significant bacterial lineage differences between BALB.B (H-2^b) and MHC congenic BALB/c (H-2^d) mice ($p < 0.05$, FDR-adjusted t test) shown as a contiguous heatmap (left) and their similarity with lineages observed in C57BL/6J mice (H-2^b) (separate heatmap at right). Mice were from the same cohort 2. Genera significantly differentially abundant between BALB/cJ and C57BL/6J ($p < 0.05$, FDR-adjusted t test) are marked in bold.

(G) Heatmap showing abundances of bacterial lineages significantly ($p < 0.05$, FDR-adjusted t test) different between MHC-sharing ex-GF C57BL/6J and BALB.B mice.

(H) Bacterial lineages with significantly ($p < 0.05$, FDR-adjusted t test) different abundances in BALB/cJ and BALB/c.Rag1^{-/-} mice. *Dehalobacterium* (bold) is also present in (G).

(I) qPCR comparison of the SFB loads in three BALB/c-based strains (BALB.B, BALB/cJ, and BALB/c.Rag1^{-/-}). Log₂ (fold change) compared to B6 was calculated as described in Experimental Model and Subject Details. Horizontal lines indicate the means of values obtained for each individual data point ± SD. Significance for real-time PCR was calculated by ordinary one-way ANOVA.

(J and K) Comparison of IgA⁺ and IgA⁻ bacteria found in ex-GF MHC congenic BALB/cJ (J) and BALB.B (K) mice transferred with the same input microbiota. Shared genera are marked in bold. Heatmaps show lineages with statistically significant differences ($p < 0.05$, FDR-adjusted t test). Error bars indicate SD.

microbiota differed from the microbiomes of control B6 recipients as expected (cohort 3; Figure 3D), but were not separable in either PCA or principal-coordinate analysis (PCoA) paired comparison (Figures 3E and S3E). Overall, MHC congenic strains carried microbiomes that were either not separable by 16S rRNA gene analyses or were closer to one another than to the microbiomes of mice from unrelated strains.

Comparison of the microbiomes of recipient BALB/c (H-2^d), BALB.B (H-2^b), and B6 (H-2^b) mice allows a simultaneous analysis of the MHC- and non-MHC-dependent control of the microbial composition of the gut. First, microbial lineages with statistically different abundances between BALB/c and BALB.B strains ($p < 0.05$, FDR-adjusted t test) were identified. Second,

their abundance in the B6 (H-2^b) mice used in the same association experiment was measured (cohort 2; Figures 3C and 3F). The pattern of significant differences in the representation of bacterial lineages between BALB/c and BALB.B mice was similar to the differences between BALB/c and B6 mice (Figure 3F). Notably, the abundances of *Holdemania*, *Mucispirillum*, and *Coprococcus* were higher in BALB.B and B6 mice ($p < 0.05$, FDR-adjusted t test) compared to BALB/c mice (Figure 3F). Thus, expansion of the listed bacteria was favored in mice of the H-2^b MHC haplotype. At the same time, some bacterial lineages differentially amplified in the microbiomes of MHC-identical B6 and BALB.B mice (Figure 3G) pointed at the influences of non-MHC genes on microbial composition.

Another way to measure the input of adaptive immunity in controlling the microbiota is to use mice lacking an adaptive immune system, such as recombination-activating gene (RAG) recombinase⁻ animals. A comparison of the microbiota of simultaneously repopulated GF BALB/c and BALB/c.*Rag1*^{-/-} mice revealed an enhanced presence of several microbial lineages, including *Holdemania* and *Coprococcus* in Rag1-deficient mice (Figure 3H). The same lineages were also enhanced in BALB.B and B6 compared to MHC-disparate BALB/c mice (Figure 3F), suggesting that the low abundance of these lineages in BALB/c mice was due to antigen-specific adaptive immune mechanisms.

Another lineage enhanced in BALB/c.*Rag1*^{-/-} mice was *Dehalobacterium* (Figure 3H). It was reduced in BALB.B mice compared to B6 that have the same MHC (Figure 3G), meaning that this bacterium's control was MHC independent. Thus, this lineage could be controlled by mechanisms that involve somatically rearranged immunoreceptors that are independent of MHC, such as receptors of NKT cells or of gamma-delta T cells.

Bacteria identified as *Candidatus* Arthromitus (also known as segmented filamentous bacteria [SFB]) presented an interesting case. SFB were more abundant in B6 than in BALB/c mice in cohort 1 (Figure 2F) (similar to a previously reported GF association experiment; Fransen et al., 2015; Figure S4A), and in BALB.B mice, this bacterium showed a trend of higher abundance compared to BALB/c mice (cohort 2; Figure S4B). Thus, we used qPCR to validate these findings and to compare SFB abundances in BALB/c, BALB.B, BALB/c.*Rag1*^{-/-}, and B6 mice from the same transfer experiment (Figure 3I). Whereas BALB.B demonstrated an SFB abundance similar to B6, both BALB/c and, most important, BALB/c.*Rag1*^{-/-} mice, had reduced abundances of this bacterium. These results suggested that the H-2^b MHC haplotype favors SFB replication. Previous publications have revealed that B6 mice mount anti-SFB responses (Th17 response [Ivanov et al., 2009] and T cell-dependent immunoglobulin A [IgA] response [Bunker et al., 2015]). BALB/c RAG-deficient mice cannot mount such responses, yet they demonstrated a paucity of SFB compared to BALB.B and B6 mice. The data led to the conclusion that SFB benefits from immune responses induced in H-2^b mice.

To test whether MHC differences affect anti-commensal IgA responses, we used the IgA sequencing (IgA-seq) method (Palm et al., 2014) to compare microbes bound by IgA in MHC congenic BALB/c and BALB.B mice. Thus, IgA⁺ and IgA⁻ microbes were sorted from the colonic contents of BALB/c and BALB.B mice colonized with the same microbiota (Figure S4C) and analyzed for 16S rRNA gene variation. Whereas the majority of IgA antibodies in the steady state recognize microbial and dietary antigens in a T cell-independent and broadly specific manner (Bunker et al., 2017), pathogens induce highly specific IgA antibodies, and some commensals are enriched in the IgA⁺ fraction when sequences of sorted IgA⁺ and IgA⁻ microbes are compared (Palm et al., 2014; Bunker et al., 2015).

Lineage variations with statistical significance ($p < 0.05$, FDR-adjusted t test) were found between the IgA⁺ and IgA⁻ fractions in mice from both strains (Figures 3J and 3K). Most IgA⁻ lineages were identical between BALB/c and BALB.B mice, whereas IgA⁺ lineages were distinct between the two congenic strains. For example, both *Mucispirillum* and SFB were found to be coated

with IgA in BALB.B mice, but they were excluded from the IgA⁺ fractions in BALB/c mice (Figures 3J and 3K). These two lineages were previously described in B6 (H-2^b) mice as stimulating production of IgA in a T cell-dependent manner (Bunker et al., 2015). Thus, our approach demonstrates that the ability to induce such IgA responses depends on the specific alleles of MHC molecules.

Finally, to define microbiota-controlling effector mechanisms that are polymorphic, we profiled gene expression in the different compartments of the guts of mice from two genetically distinct backgrounds. We isolated RNA from three regions of the gut (duodenum + jejunum, DJ; ileum, I; and colon, C) of ex-GF B6 and BALB/c mice from cohort 2 and used it for RNA sequencing (RNA-seq) analysis. Variation in gene expression between the two strains was obvious in all three regions of the gut (Figure 4A), and, as expected, the gene expression profiles were distinct between the regions of the gut (Figures 4B and 4C).

Significant gene expression differences between B6 and BALB/cJ strains were identified using both log₂ fold change (detected at >1 transcript per million [TPM]) and $p < 0.05$ (FDR-adjusted t test). The expression of both adaptive and innate immunity genes showed strain-specific variations (Figure S5). B6 and BALB/cJ mice used distinct sets of Ig V_H and V_L genes. However, this polymorphism is not uniquely linked to anti-microbial antibodies (Collins et al., 2015).

Aside from adaptive immunity genes, the functions of the remaining host genes differentially expressed in BALB/c and B6 mice were analyzed using Gene Ontology (GO) (Ashburner et al., 2000). We were specifically interested in differentially expressed genes with functions that may regulate intestinal homeostasis. Two broad functional categories of genes differentially expressed in the intestinal compartments of B6 and BALB/c mice were identified. The first group included genes supporting a wide range of innate immune functions, including negative regulators of peptidase activity (Serpin A family members), complement proteins, interferon-stimulated genes, an inflammasome component, pentraxins, and osteopontin (Figure 4B). The detailed description of the genes in this eclectic group is shown in Table S2. The second large group of discordant genes included antimicrobial peptides—defensins alpha (*Defa*) (Figure 4C). The complete list of genes with significantly different expression between B6 and BALB/c mice is shown in Table S3.

DISCUSSION

Overall, the results of our studies demonstrate that when the living environment of the animal is strictly controlled, including controlled microbial repopulation, the influences of host genetics on microbial composition could be detected and studied. We have compared the microbiomes of post-pubescent G1 mice, the progeny of the microbiota recipient G0 mice of different genetic backgrounds. This strategy allowed us to analyze stabilized commensal communities after they have been shaped by pregnancy, transfer to newborns, early infancy, and exposure to milk and solid food. Recently demonstrated genetic variations, such as *Tlr5* deficiency (Fulde et al., 2018) affected the microbiota composition in neonatal mice more strongly than in adults, supporting our choice of the experimental protocol.

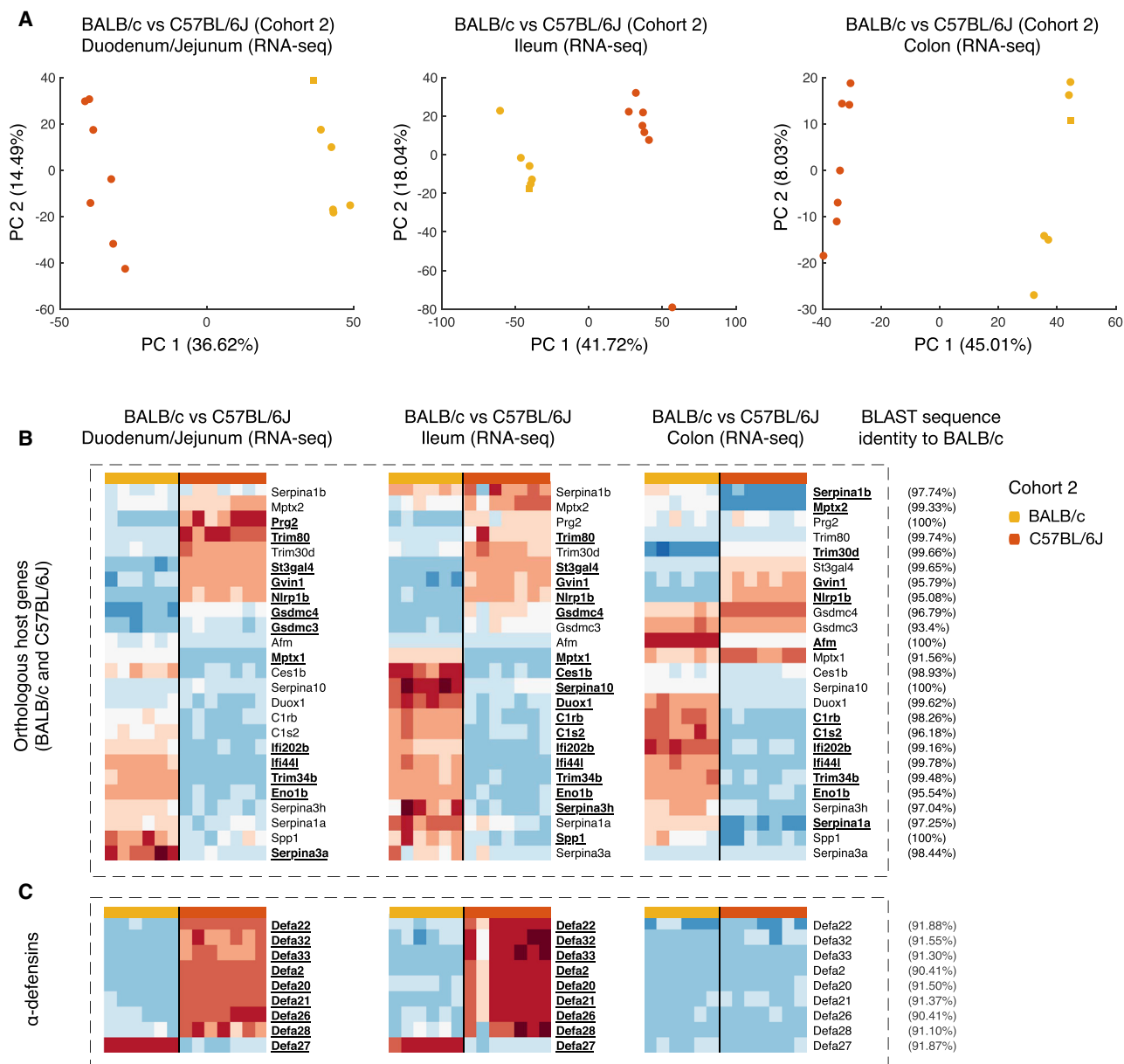


Figure 4. Polymorphic Gene Expression in the Intestinal Compartments of Ex-GF C57BL/6J and BALB/cJ Mice Colonized with the Same Microbiota (Cohort 2)

(A) PCA of RNA-seq data generated from different intestinal compartments from the two mouse strains. A total of 6 BALB/c and 7 C57BL/6 mice were used. (B) Heatmaps showing significant ($p < 0.05$, FDR-adjusted t test) differences in gene expression identified between the two strains using log₂ fold change as a readout. Gene names in bold reflect statistical significance in a specific compartment. (C) Differences in the expression of defensins alpha between mice from the two strains. BLAST sequence similarity of BALB/c sequence and C57BL/6J reference gene sequence is indicated at right.

Unambiguously, the input microbiota strongly determined the resultant microbiota in its recipients (Figures 1B and 2F–2I). For instance, comparison of the microbiota of B6 and BALB/c repopulated ex-GF mice from different colonization experiments identified several common lineages, such as *Turicibacter*, *Clostridiaceae*, and *Peptostreptococcaceae* differentially abundant in cohorts 1 and 3 (Figures 2F and 2G), but not in cohort 2 (Figure 2H). These results were explained by the lack of *Turicibacter*

and *Peptostreptococcaceae* lineages in the donor microbiota used to repopulate mice in cohort 2 (Figure 2I). Bacteria from the *Clostridiaceae* family found in mice from cohort 2 did not show differential abundance in recipient BALB/c and B6 microbiota (Figure 2I). That was most likely due to the presence of different members of the *Clostridiaceae* family in mice from cohort 2 compared to mice from cohorts 1 and 3. We have also processed the data from a previously published experiment

(Fransen et al., 2015), in which the bacterial species of ex-GF B6 and BALB/c adult GF recipient mice associated with the B6 microbiota were compared at 8 weeks post-transfer. We found that the differential abundance of bacterial lineages between BALB/cJ and B6 mice described in that study did not overlap with our results (Figure S4A), supporting the point that the input microbiota defines the output results in the transfer studies. These results suggest that the only way to overcome the legacy effects is to compare microbiomes of mice within the same transfer experiment.

Using congenic and gene-targeted GF mice, it is possible to detect microbial lineages that are controlled by different types of immune mechanisms. MHC congenic GF mouse strains are a valuable tool to address the role of adaptive immune mechanisms in the control of microbial composition. Although it was previously suggested that mice with different MHC alleles may have distinct microbial compositions (Kubinak et al., 2015), the experimental setup used could not exclude the influence of input variations on the results. By excluding input variations, we were able to detect MHC-dependent microbial shifts in two of three congenic mouse strain combinations tested (Figures 3B, 3D, and 3E). Whereas the microbiomes of MHC congenic strains on the BALB/c genetic background carrying H-2ⁱ, H-2^b, and H-2^d haplotypes were separable by PCA (Figures 3B and 3C) or PCoA (Figures S3C and S3D) analyses, the microbiomes of the I/LnJ MHC congenic strains (H-2ⁱ versus H-2^h) were not (Figures 3E and S3E). Furthermore, the overall distances between the microbiomes of BALB/c MHC congenic mice were smaller than the distances between the microbiomes of the strains of completely different backgrounds (Figure 3A). Although such experiments should be repeated using frozen aliquoted microbiota stocks or defined microbial communities, our experiments suggested that the role of MHC-dependent adaptive immunity in shaping the gut microbiota is somewhat limited and is likely reserved for specific colonizers, such as pathogens, or intrusive commensals, such as SFB (Ladinsky et al., 2019).

Adaptive immune receptors require RAG recombinases for their rearrangements, and thus, RAG-deficient mice are free of adaptive immunity. RAG-deficient mice lack alpha-beta T cells, gamma-delta T cells, and NKT cells, as their invariable T cell receptor α (TCR- α) chains require RAG-dependent somatic gene rearrangement. Human gamma-delta T cells were shown to recognize alkylamines from *Proteus* species (Bukowski et al., 1999). Coincidentally, *Proteus* was enhanced in RAG-deficient mice compared to RAG-sufficient mice (Figure 3H). NKT cells were shown to regulate the production of anti-microbial peptides by Paneth cells (Farin et al., 2014). We found that *Dehalobacterium* was significantly enhanced in RAG-deficient mice compared to RAG-sufficient mice (Figure 3H). We have also analyzed the data from a previous study describing the microbiota of CD1d-deficient mice (lacking NKT cells) (Selvanantham et al., 2016) and found that *Dehalobacterium* was enhanced in these mice ($p = 0.015$). These data suggest that NKT cells could control *Dehalobacterium* by regulating the production of anti-microbial peptides.

Analysis of RAG-deficient mice has also led to some unexpected results. We found that BALB/c mice had significantly less SFB compared to mice from the B6 and BALB.B strains (Fig-

ure 3I). SFB was also found to be more abundant in B6 mice compared to BALB/c mice in a previously published dataset that we have analyzed (Fransen et al., 2015; Figure S4A). This result could be explained by an ability of the H-2^d but not the H-2^b allele to mount a strong anti-SFB response. However, the lack of SFB expansion in BALB/c RAG-deficient mice indicates that the specific immune response is likely promoting SFB survival. In agreement with that, we found that BALB.B (H-2^b) mice mounted stronger IgA responses to SFB compared to BALB/c (H-2^d) mice (Figure 3I). A beneficial role of IgAs for some microbes has been recently demonstrated (Donaldson et al., 2018), but the dependence of this response on the specific MHC haplotypes (and hence on adaptive immunity) has not been documented. It could also be argued that IgA suppresses SFB as it is enhanced in activation-induced cytidine deaminase⁻ (AID⁻) mice (which cannot class switch their Igs) compared to AID⁺ mice (Suzuki et al., 2004). However, AID-deficient mice demonstrate microbe-independent spontaneous inflammation in the gut (Hase et al., 2008), which could activate the ileal epithelium to produce factors promoting SFB expansion. At present, we have no direct evidence to determine whether IgA responses or anti-SFB T cell responses (Ivanov et al., 2009) promote SFB in B6 mice. However, the fact that SFB enables a specific type of endocytosis to produce vesicles loaded with a T cell-inducing antigen, and its importance for Th17 activation (Ladinsky et al., 2019), suggest that the activation of immune responses by SFB in general could be an adaptation evolved by this bacterium for its own benefit.

A number of other bacterial lineages were preferentially coated by IgA in BALB.B mice (Figure 3J), including *Mucispirillum*, which was previously demonstrated to induce a T cell-dependent IgA response (Bunker et al., 2015). Thus, it is possible that bacteria other than SFB could also enhance their replication in mice with specific MHC haplotypes by stimulating IgA responses against themselves.

In addition to adaptive immunity, multiple innate mechanisms may control the microbiota composition. These innate mechanisms may be immune or metabolic in nature, or they may control aspects of intestinal physiology such as motility and acidity. To identify innate polymorphic mechanisms operating in the gut, we profiled gene expression (using RNA-seq) in three intestinal compartments from B6 and BALB/c mice populated with the same input microbiota (Figure 4; Tables S2 and S3). Among the polymorphic innate factors, we found a family of antimicrobial peptides, defensins alpha (Defa), which differ in expression between mouse strains and between the regions of the gut (Volynets et al., 2016; Karlsson et al., 2008; Shanahan et al., 2011). Since RNA-seq reads are tested against a reference B6 genome, some genes that are either deleted or too different between B6 and BALB/c mice may not be properly identified. In fact, Defa sequence identity was lower than the sequence identity of the other genes among BALB/c and B6 genomes (Figure 4C) (Zerbino et al., 2018). Defa show some degree of anti-microbial specificity (Salzman et al., 2010). Thus, the highly variable array of defensins could be one of the genetically polymorphic forces shaping the commensal repertoire.

Overall, it can be concluded that genetic backgrounds shape input microbial repertoires in their own idiosyncratic fashion.

However, we find it remarkable that the host-determined polymorphic influences on microbial composition are limited in scope and target only select microbial lineages (Figure S6). That implies that total control over the enormous body of microorganisms by the host immunity is unlikely (probably due to its extremely high cost) and that both non-polymorphic control mechanisms and other natural forces could be involved. Despite the significant evolutionary restriction of the variety of commensal bacterial phyla compared to free-living microbes (Dethlefsen et al., 2007), gut commensals must still follow the general rules of initial colonization and assembly found in other ecological systems (e.g., substrate attachment, establishment of the redox cascades, interdependence of the members), which may function in the mammalian host without its direct control.

We expect that further carefully arranged and controlled studies of genetically modified gnotobiotic animals using engineered communities of different complexities will elucidate the input of individual genetic mechanisms in host-commensal symbiosis.

STAR★METHODS

Detailed methods are provided in the online version of this paper and include the following:

- KEY RESOURCES TABLE
- LEAD CONTACT AND MATERIALS AVAILABILITY
- EXPERIMENTAL MODEL AND SUBJECT DETAILS
 - Mouse lines
- METHOD DETAILS
 - Monitoring sterility in gnotobiotic isolators
 - Transfer of gastrointestinal microbiota
 - DNA extraction, 16S rRNA amplicon sequencing and analysis
 - RNA isolation, sequencing (RNASeq), and analysis
 - Purification of IgA-coated and uncoated bacteria from colons
 - Real-time quantitative PCR
- QUANTIFICATION AND STATISTICAL ANALYSIS
- DATA AND CODE AVAILABILITY

SUPPLEMENTAL INFORMATION

Supplemental Information can be found online at <https://doi.org/10.1016/j.celrep.2019.09.010>.

ACKNOWLEDGMENTS

We thank Dr. Andre Ouellette (University of Southern California, Los Angeles, CA) for helpful discussion and Drs. Maria Rescigno, Bruno Fosso (Universita' di Milano, Milan, Italy), and Thierry Mallevaey (University of Toronto, Toronto, ON, Canada) for sharing their primary sequencing data. A.C. is supported by NIH grants R01AI082418 and R01AI127411. A.C. and R.d.P. are supported by Department of Defense (DOD) grant W911NF-17-1-0402. A.C. is supported by NIH R01AI082418. T.G. was supported by NIH grant R01AI090084. L.Y. and J.M.P. were supported by NIH T32 GM007183 and T32 AI065382, respectively. This work was also supported by NIH/NIDDK Digestive Disease Research Core Center grant DK42086 and by NIH grant P30 CA014599.

AUTHOR CONTRIBUTIONS

A.A.K. performed the computational analysis of the data and wrote the manuscript. L.Y. and J.M.P. performed the mouse experiments. R.d.P. performed the IgA-seq and the qPCR experiments. D.A.A. oversaw the DNA library preparations and the high-throughput sequencing, and performed the primary data analysis. K.O. performed the RNA-seq. T.G. and A.C. conceived and oversaw the project and wrote the manuscript.

DECLARATION OF INTERESTS

The authors declare no competing interests.

Received: January 22, 2019

Revised: July 28, 2019

Accepted: September 4, 2019

Published: October 15, 2019

SUPPORTING CITATIONS

Brodziak et al., 2013; Chen et al., 2014; Costa et al., 2018; Grasberger et al., 2013; Haber et al., 2017; Han et al., 2013; Hosokawa, 2008; Huang et al., 2015; MacMicking, 2004; Mihara et al., 2016; Ozato et al., 2008; Toyonaga et al., 2015; van der Meer-van Kraaij et al., 2007; Wang et al., 2011; Williams et al., 2015; Yuan et al., 2018.

REFERENCES

- Ashburner, M., Ball, C.A., Blake, J.A., Botstein, D., Butler, H., Cherry, J.M., Davis, A.P., Dolinski, K., Dwight, S.S., Eppig, J.T., et al.; The Gene Ontology Consortium (2000). Gene ontology: tool for the unification of biology. *Nat. Genet.* 25, 25–29.
- Bacchetti De Gregoris, T., Aldred, N., Clare, A.S., and Burgess, J.G. (2011). Improvement of phylum- and class-specific primers for real-time PCR quantification of bacterial taxa. *J. Microbiol. Methods* 86, 351–356.
- Barman, M., Unold, D., Shifley, K., Amir, E., Hung, K., Bos, N., and Salzman, N. (2008). Enteric salmonellosis disrupts the microbial ecology of the murine gastrointestinal tract. *Infect. Immun.* 76, 907–915.
- Belkaid, Y., and Hand, T.W. (2014). Role of the microbiota in immunity and inflammation. *Cell* 157, 121–141.
- Bray, N.L., Pimentel, H., Melsted, P., and Pachter, L. (2016). Near-optimal probabilistic RNA-seq quantification. *Nat. Biotechnol.* 34, 525–527.
- Brodziak, F., Meharg, C., Blaut, M., and Loh, G. (2013). Differences in mucosal gene expression in the colon of two inbred mouse strains after colonization with commensal gut bacteria. *PLoS One* 8, e72317.
- Bukowski, J.F., Morita, C.T., and Brenner, M.B. (1999). Human gamma delta T cells recognize alkylamines derived from microbes, edible plants, and tea: implications for innate immunity. *Immunity* 11, 57–65.
- Bunker, J.J., Flynn, T.M., Koval, J.C., Shaw, D.G., Meisel, M., McDonald, B.D., Ishizuka, I.E., Dent, A.L., Wilson, P.C., Jabri, B., et al. (2015). Innate and Adaptive Humoral Responses Coat Distinct Commensal Bacteria with Immunoglobulin A. *Immunity* 43, 541–553.
- Bunker, J.J., Erickson, S.A., Flynn, T.M., Henry, C., Koval, J.C., Meisel, M., Jabri, B., Antonopoulos, D.A., Wilson, P.C., and Bendelac, A. (2017). Natural polyreactive IgA antibodies coat the intestinal microbiota. *Science* 358, eaan6619.
- Caporaso, J.G., Bittinger, K., Bushman, F.D., DeSantis, T.Z., Andersen, G.L., and Knight, R. (2010a). PyNAST: a flexible tool for aligning sequences to a template alignment. *Bioinformatics* 26, 266–267.
- Caporaso, J.G., Kuczynski, J., Stombaugh, J., Bittinger, K., Bushman, F.D., Costello, E.K., Fierer, N., Peña, A.G., Goodrich, J.K., Gordon, J.I., et al. (2010b). QIIME allows analysis of high-throughput community sequencing data. *Nat. Methods* 7, 335–336.

- Caporaso, J.G., Lauber, C.L., Walters, W.A., Berg-Lyons, D., Huntley, J., Fierer, N., Owens, S.M., Betley, J., Fraser, L., Bauer, M., et al. (2012). Ultra-high-throughput microbial community analysis on the Illumina HiSeq and MiSeq platforms. *ISME J.* 6, 1621–1624.
- Carmody, R.N., Gerber, G.K., Luevano, J.M., Jr., Gatti, D.M., Somes, L., Svenson, K.L., and Turnbaugh, P.J. (2015). Diet dominates host genotype in shaping the murine gut microbiota. *Cell Host Microbe* 17, 72–84.
- Chen, S., Duan, G., Zhang, R., and Fan, Q. (2014). *Helicobacter pylori* cytotoxin-associated gene A protein upregulates α -enolase expression via Src/MEK/ERK pathway: implication for progression of gastric cancer. *Int. J. Oncol.* 45, 764–770.
- Collins, A.M., Wang, Y., Roskin, K.M., Marquis, C.P., and Jackson, K.J. (2015). The mouse antibody heavy chain repertoire is germline-focused and highly variable between inbred strains. *Philos. Trans. R. Soc. Lond. B Biol. Sci.* 370, 20140236.
- Costa, N.A., Gut, A.L., Azevedo, P.S., Polegato, B.F., Magalhães, E.S., Ishikawa, L.L.W., Bruder, R.C.S., Silva, E.A.D., Gonçalves, R.B., Tanni, S.E., et al. (2018). Peptidylarginine deiminase 4 concentration, but not PADI4 polymorphisms, is associated with ICU mortality in septic shock patients. *J. Cell. Mol. Med.* 22, 4732–4737.
- David, L.A., Materna, A.C., Friedman, J., Campos-Baptista, M.I., Blackburn, M.C., Perrotta, A., Erdman, S.E., and Alm, E.J. (2014). Host lifestyle affects human microbiota on daily timescales. *Genome Biol.* 15, R89.
- Dethlefsen, L., McFall-Ngai, M., and Relman, D.A. (2007). An ecological and evolutionary perspective on human-microbe mutualism and disease. *Nature* 449, 811–818.
- Donaldson, G.P., Ladinsky, M.S., Yu, K.B., Sanders, J.G., Yoo, B.B., Chou, W.C., Conner, M.E., Earl, A.M., Knight, R., Bjorkman, P.J., and Mazmanian, S.K. (2018). Gut microbiota utilize immunoglobulin A for mucosal colonization. *Science* 360, 795–800.
- Edgar, R.C. (2010). Search and clustering orders of magnitude faster than BLAST. *Bioinformatics* 26, 2460–2461.
- Elinav, E., Henao-Mejia, J., Strowig, T., and Flavell, R. (2018). NLRP6 and Dysbiosis: Avoiding the Luring Attraction of Over-Simplification. *Immunity* 48, 603–604.
- Farin, H.F., Karthaus, W.R., Kujala, P., Rakhshandehroo, M., Schwank, G., Vries, R.G., Kalkhoven, E., Nieuwenhuis, E.E., and Clevers, H. (2014). Paneth cell extrusion and release of antimicrobial products is directly controlled by immune cell-derived IFN- γ . *J. Exp. Med.* 217, 1393–1405.
- Fransen, F., Zagato, E., Mazzini, E., Fosso, B., Manzari, C., El Aidy, S., Chiavelli, A., D'Erchia, A.M., Sethi, M.K., Pabst, O., et al. (2015). BALB/c and C57BL/6 Mice Differ in Polyreactive IgA Abundance, which Impacts the Generation of Antigen-Specific IgA and Microbiota Diversity. *Immunity* 43, 527–540.
- Fulde, M., Sommer, F., Chassaing, B., van Vorst, K., Dupont, A., Hensel, M., Basic, M., Klopffleisch, R., Rosenstiel, P., Bleich, A., et al. (2018). Neonatal selection by Toll-like receptor 5 influences long-term gut microbiota composition. *Nature* 560, 489–493.
- Goodrich, J.K., Waters, J.L., Poole, A.C., Sutter, J.L., Koren, O., Blekhman, R., Beaumont, M., Van Treuren, W., Knight, R., Bell, J.T., et al. (2014). Human genetics shape the gut microbiome. *Cell* 159, 789–799.
- Goodrich, J.K., Davenport, E.R., Beaumont, M., Jackson, M.A., Knight, R., Ober, C., Spector, T.D., Bell, J.T., Clark, A.G., and Ley, R.E. (2016). Genetic Determinants of the Gut Microbiome in UK Twins. *Cell Host Microbe* 19, 731–743.
- Grasberger, H., El-Zaatari, M., Dang, D.T., and Merchant, J.L. (2013). Dual oxidases control release of hydrogen peroxide by the gastric epithelium to prevent *Helicobacter felis* infection and inflammation in mice. *Gastroenterology* 145, 1045–1054.
- Haber, A.L., Biton, M., Rogel, N., Herbst, R.H., Shekhar, K., Smillie, C., Burgin, G., Delorey, T.M., Howitt, M.R., Katz, Y., et al. (2017). A single-cell survey of the small intestinal epithelium. *Nature* 551, 333–339.
- Han, N.Y., Choi, W., Park, J.M., Kim, E.H., Lee, H., and Hahm, K.B. (2013). Label-free quantification for discovering novel biomarkers in the diagnosis and assessment of disease activity in inflammatory bowel disease. *J. Dig. Dis.* 14, 166–174.
- Hase, K., Takahashi, D., Ebisawa, M., Kawano, S., Itoh, K., and Ohno, H. (2008). Activation-induced cytidine deaminase deficiency causes organ-specific autoimmune disease. *PLoS One* 3, e3033.
- Hosokawa, M. (2008). Structure and catalytic properties of carboxylesterase isozymes involved in metabolic activation of prodrugs. *Molecules* 13, 412–431.
- Huang, Y.L., Chassard, C., Hausmann, M., von Itzstein, M., and Hennot, T. (2015). Sialic acid catabolism drives intestinal inflammation and microbial dysbiosis in mice. *Nat. Commun.* 6, 8141.
- Ivanov, I.I., Atarashi, K., Manel, N., Brodie, E.L., Shima, T., Karaoz, U., Wei, D., Goldfarb, K.C., Santee, C.A., Lynch, S.V., et al. (2009). Induction of intestinal Th17 cells by segmented filamentous bacteria. *Cell* 139, 485–498.
- Karlsson, J., Pütsep, K., Chu, H., Kays, R.J., Bevins, C.L., and Andersson, M. (2008). Regional variations in Paneth cell antimicrobial peptide expression along the mouse intestinal tract. *BMC Immunol.* 9, 37.
- Kubinak, J.L., Stephens, W.Z., Soto, R., Petersen, C., Chiaro, T., Gogokhia, L., Bell, R., Ajami, N.J., Petrosino, J.F., Morrison, L., et al. (2015). MHC variation sculpts individualized microbial communities that control susceptibility to enteric infection. *Nat. Commun.* 6, 8642.
- Ladinsky, M.S., Araujo, L.P., Zhang, X., Veltri, J., Galan-Diez, M., Soualhi, S., Lee, C., Irie, K., Pinker, E.Y., Narushima, S., et al. (2019). Endocytosis of commensal antigens by intestinal epithelial cells regulates mucosal T cell homeostasis. *Science* 363, eaat4042.
- Ley, R.E., Bäckhed, F., Turnbaugh, P., Lozupone, C.A., Knight, R.D., and Gordon, J.I. (2005). Obesity alters gut microbial ecology. *Proc. Natl. Acad. Sci. USA* 102, 11070–11075.
- MacMicking, J.D. (2004). IFN-inducible GTPases and immunity to intracellular pathogens. *Trends Immunol.* 25, 601–609.
- McDonald, D., Price, M.N., Goodrich, J., Nawrocki, E.P., DeSantis, T.Z., Probst, A., Andersen, G.L., Knight, R., and Hugenholtz, P. (2012). An improved Greengenes taxonomy with explicit ranks for ecological and evolutionary analyses of bacteria and archaea. *ISME J.* 6, 610–618.
- Mihara, E., Hirai, H., Yamamoto, H., Tamura-Kawakami, K., Matano, M., Kikuchi, A., Sato, T., and Takagi, J. (2016). Active and water-soluble form of lipidated Wnt protein is maintained by a serum glycoprotein afamin/ α -albumin. *eLife* 5, e11621.
- Ozato, K., Shin, D.M., Chang, T.H., and Morse, H.C., 3rd. (2008). TRIM family proteins and their emerging roles in innate immunity. *Nat. Rev. Immunol.* 8, 849–860.
- Palm, N.W., de Zoete, M.R., Cullen, T.W., Barry, N.A., Stefanowski, J., Hao, L., Degnan, P.H., Hu, J., Peter, I., Zhang, W., et al. (2014). Immunoglobulin A coating identifies colitogenic bacteria in inflammatory bowel disease. *Cell* 158, 1000–1010.
- Rawls, J.F., Mahowald, M.A., Ley, R.E., and Gordon, J.I. (2006). Reciprocal gut microbiota transplants from zebrafish and mice to germ-free recipients reveal host habitat selection. *Cell* 127, 423–433.
- Rothschild, D., Weissbrod, O., Barkan, E., Kurilshikov, A., Korem, T., Zeevi, D., Costea, P.I., Godneva, A., Kalka, I.N., Bar, N., et al. (2018). Environment dominates over host genetics in shaping human gut microbiota. *Nature* 555, 210–215.
- Salzman, N.H., Hung, K., Haribhai, D., Chu, H., Karlsson-Sjöberg, J., Amir, E., Teggatz, P., Barman, M., Hayward, M., Eastwood, D., et al. (2010). Enteric defensins are essential regulators of intestinal microbial ecology. *Nat. Immunol.* 11, 76–83.
- Selvanantham, T., Lin, Q., Guo, C.X., Surendra, A., Fieve, S., Escalante, N.K., Guttman, D.S., Streutker, C.J., Robertson, S.J., Philpott, D.J., and Mallevaey, T. (2016). NKT Cell-Deficient Mice Harbor an Altered Microbiota That Fuels Intestinal Inflammation during Chemically Induced Colitis. *J. Immunol.* 197, 4464–4472.

- Shanahan, M.T., Tanabe, H., and Ouellette, A.J. (2011). Strain-specific polymorphisms in Paneth cell α -defensins of C57BL/6 mice and evidence of vestigial myeloid α -defensin pseudogenes. *Infect. Immun.* *79*, 459–473.
- Sonnenburg, E.D., Smits, S.A., Tikhonov, M., Higginbottom, S.K., Wingreen, N.S., and Sonnenburg, J.L. (2016). Diet-induced extinctions in the gut microbiota compound over generations. *Nature* *529*, 212–215.
- Storey, J.D. (2002). A direct approach to false discovery rates. *J. R. Stat. Soc. B* *64*, 479–498.
- Suzuki, K., Meek, B., Doi, Y., Muramatsu, M., Chiba, T., Honjo, T., and Fagarasan, S. (2004). Aberrant expansion of segmented filamentous bacteria in IgA-deficient gut. *Proc. Natl. Acad. Sci. USA* *101*, 1981–1986.
- Toyonaga, T., Nakase, H., Ueno, S., Matsuura, M., Yoshino, T., Honzawa, Y., Itou, A., Namba, K., Minami, N., Yamada, S., et al. (2015). Osteopontin Deficiency Accelerates Spontaneous Colitis in Mice with Disrupted Gut Microbiota and Macrophage Phagocytic Activity. *PLoS One* *10*, e0135552.
- Turner, S., Pryer, K.M., Miao, V.P., and Palmer, J.D. (1999). Investigating deep phylogenetic relationships among cyanobacteria and plastids by small subunit rRNA sequence analysis. *J. Eukaryot. Microbiol.* *46*, 327–338.
- van der Meer-van Kraaij, C., Siezen, R., Kramer, E., Reinders, M., Blokzijl, H., van der Meer, R., and Keijzer, J. (2007). Dietary modulation and structure prediction of rat mucosal pentraxin (Mptx) protein and loss of function in humans. *Genes Nutr.* *2*, 275–285.
- Volynets, V., Rings, A., Bárdos, G., Ostaff, M.J., Wehkamp, J., and Bischoff, S.C. (2016). Intestinal barrier analysis by assessment of mucins, tight junctions, and α -defensins in healthy C57BL/6J and BALB/cJ mice. *Tissue Barriers* *4*, e1208468.
- Walters, W., Hyde, E.R., Berg-Lyons, D., Ackermann, G., Humphrey, G., Parada, A., Gilbert, J.A., Jansson, J.K., Caporaso, J.G., Fuhrman, J.A., et al. (2015). Improved Bacterial 16S rRNA Gene (V4 and V4-5) and Fungal Internal Transcribed Spacer Marker Gene Primers for Microbial Community Surveys. *mSystems*, Published online December 22, 2015. <https://doi.org/10.1128/mSystems.00009-15>.
- Wang, Z., Klipfell, E., Bennett, B.J., Koeth, R., Levison, B.S., Dugar, B., Feldstein, A.E., Britt, E.B., Fu, X., Chung, Y.M., et al. (2011). Gut flora metabolism of phosphatidylcholine promotes cardiovascular disease. *Nature* *472*, 57–63.
- Williams, T.M., Leeth, R.A., Rothschild, D.E., Coutermarsh-Ott, S.L., McDaniel, D.K., Simmons, A.E., Heid, B., Cecere, T.E., and Allen, I.C. (2015). The NLRP1 inflammasome attenuates colitis and colitis-associated tumorigenesis. *J. Immunol.* *194*, 3369–3380.
- Wullaert, A., Lamkanfi, M., and McCoy, K.D. (2018). Defining the Impact of Host Genotypes on Microbiota Composition Requires Meticulous Control of Experimental Variables. *Immunity* *48*, 605–607.
- Yuan, Y.Y., Xie, K.X., Wang, S.L., and Yuan, L.W. (2018). Inflammatory caspase-related pyroptosis: mechanism, regulation and therapeutic potential for inflammatory bowel disease. *Gastroenterol. Rep. (Oxf.)* *6*, 167–176.
- Yurkovetskiy, L., Burrows, M., Khan, A.A., Graham, L., Volchkov, P., Becker, L., Antonopoulos, D., Umesaki, Y., and Chervonsky, A.V. (2013). Gender bias in autoimmunity is influenced by microbiota. *Immunity* *39*, 400–412.
- Zerbino, D.R., Achuthan, P., Akanni, W., Amode, M.R., Barrell, D., Bhai, J., Billis, K., Cummins, C., Gall, A., Girón, C.G., et al. (2018). Ensembl 2018. *Nucleic Acids Res.* *46* (D1), D754–D761.

STAR★METHODS

KEY RESOURCES TABLE

REAGENT or RESOURCE	SOURCE	IDENTIFIER
Antibodies		
Normal goat serum	Jackson ImmunoResearch	Cat#005-000-121; RRID:AB_2336990
Goat anti-mouse IgA	SouthernBiotech	Cat#1040-01; RRID:AB_2314669
Goat anti-mouse IgA-biotin	SouthernBiotech	Cat#1040-08; RRID:AB_2794374
Chemicals, Peptides, and Recombinant Proteins		
Protease inhibitor cocktail	Roche	Cat#11626400
SYTO-13	Life Technologies	Cat#S7575
Critical Commercial Assays		
DNeasy PowerSoil HTP 96 Kit	QIAGEN	Cat#12955-4
5 PRIME HotMaster Mix kit	Quantabio	Cat# 2200410
UltraClean 96 PCR Cleanup Kit	QIAGEN	Cat#12596-4
Quant-iT PicoGreen dsDNA Assay Kit	Invitrogen/Thermo Fisher Scientific	Cat# P11496
PureLink RNA Mini Kit	Thermo Fisher Scientific	Cat#12183018A
TotalRNA TruSEQ kits RiboZero depletion	Illumina	Cat# 20020599
SYBR Green master mix	Thermo Fisher Scientific	Cat#4364346
Deposited Data		
RNA-seq data	This paper	GEO: GSE136572
16S data	This paper	Github: https://github.com/akds/microbiome-MHC
16S dataset	Selvanantham et al., 2016	OTU table from authors
16S dataset	Fransen et al., 2015	OTU table from authors
Experimental Models: Organisms/Strains		
Mouse: I/LnJ	The Jackson Laboratory	JAX:000674
Mouse: C57BL/6J (B6)	The Jackson Laboratory	JAX:000664
Mouse: BALB/cJ	The Jackson Laboratory	JAX:000651
Mouse: C.B10-H2 ^b /J ^{lilMcdJ}	The Jackson Laboratory	JAX:001952
Mouse: C.129S7(B6)-Rag1tm1Mom/J	The Jackson Laboratory	JAX: 003145
Mouse: C57BL/6NTac	Taconic Biosciences	B6NTac
Mouse: C3H/HeN	Dr. T. Golovkina University of Chicago	N/A
Mouse: BALB/cJ-H-2 ^J	Dr. T. Golovkina University of Chicago	N/A
Mouse: I/LnJ-H-2 ^k	Dr. T. Golovkina University of Chicago	N/A
Mouse: Germ-free I/LnJ	Dr. T. Golovkina University of Chicago	N/A
Mouse: Germ-free BALB/cJ	Dr. T. Golovkina University of Chicago	N/A
Mouse: Germ-free C3H/HeN	Dr. T. Golovkina University of Chicago	N/A
Mouse: Germ-free BALB/cJ-H-2 ^J	Dr. T. Golovkina University of Chicago	N/A
Mouse: Germ-free I/LnJ-H-2 ^k	Dr. T. Golovkina University of Chicago	N/A
Mouse: Germ-free C57BL/6J (B6)	Dr. E. Chang, University of Chicago	N/A
Oligonucleotides		
Real-time forward PCR primer for SFB, SFB736F GACGCTGAGGCATGAGAGCAT	Barman et al., 2008	N/A
Real-time reverse PCR primer for SFB, SFB844R GACGGCACGGATTGTTATTCA	Barman et al., 2008	N/A

(Continued on next page)

Continued		
REAGENT or RESOURCE	SOURCE	IDENTIFIER
Real-time forward PCR primer for 16S rRNA genes, Uni 926F AAACTCAAAGAATTGACGG	Bacchetti De Gregoris et al., 2011	N/A
Real-time reverse PCR primer for 16S rRNA genes, Uni 1062R CTCACRRACGAGCTGAC	Bacchetti De Gregoris et al., 2011	N/A
Forward PCR primer to monitor sterility in GF isolators, 8F AGAGTTTGATCCTGGCTCAG	Turner et al., 1999	N/A
Reverse PCR primer to monitor sterility in GF isolators, 1391R GACGGGCGGTGWGTRCA	Turner et al., 1999	N/A
Software and Algorithms		
QIIME 1.9 analysis pipeline	Caporaso et al., 2010b	http://qiime.org/
PyNASt	Caporaso et al., 2010a	https://biocore.github.io/pynast/
UCLUST	Edgar, 2010	http://www.drive5.com/usearch/
MATLAB software package 9.3 (R2017b)	MathWorks	https://www.mathworks.com/products/matlab.html
Kallisto	Bray et al., 2016	https://pachterlab.github.io/kallisto/
Prism 8	GraphPad	https://www.graphpad.com/scientific-software/prism/
Other		
Streptavidin-APC	Biolegend	Cat#405207

LEAD CONTACT AND MATERIALS AVAILABILITY

Further information and requests for resources and reagents should be directed to and will be fulfilled by the lead contact Alexander Chervonsky (ahervon@bsd.uchicago.edu). This study did not generate new unique reagents.

EXPERIMENTAL MODEL AND SUBJECT DETAILS

Mouse lines

Specific pathogen free (SPF) mice

C57BL6/J (B6), I/LnJ, BALB/cJ, C.B10-H2^b/LlMcdJ (BALB/c mice with the H2^b MHC locus derived from B6 mice, a.k.a BALB.B) and C.129S7(B6)-Rag1^{tm1Mom}/J (BALB/c RAG1^{-/-}) mice were purchased from The Jackson Laboratory (Bar Harbor, ME). B6NTac were purchased from Taconic Biosciences, Inc (Rensselaer, NY). C3H/HeN mice originally obtained from the National Cancer Institute Frederick Cancer Research Facility (Frederick, MD) were maintained in our mouse colony at The University of Chicago.

To generate the BALB/cJ-H-2^J and I/LnJ-H-2^K congenic lines, BALB/cJ or I/LnJ mice were crossed to I/LnJ and C3H/HeN mice, respectively. F1 mice were then backcrossed to parental BALB/cJ or I/LnJ mice and resulting N2 females were genotyped with the markers on Chromosome 17 at 33.9 and 34.3 Mb flanking the MHC locus (Figure S2). BALB/cJ mice inheriting the I/LnJ MHC locus and I/LnJ mice inheriting the C3H/HeN MHC locus were backcrossed to BALB/cJ mice and I/LnJ, respectively, to produced N3 mice. At each generation, only those offspring that had acquired I/LnJ (for BALB/cJ-H-2^J line) or C3H/HeN (for I/LnJ-H-2^K line) MHC locus were selected for the next round of backcrossing. Two 10th-generation BALB/cJ carriers of the I/LnJ and I/LnJ carriers of the C3H/HeN MHC locus were intercrossed, and offspring homozygous for MHC locus were selected to continue the line through brother-sister mating. All animals were housed at The University of Chicago SPF facility.

The studies described here have been reviewed and approved by the Animal Care and Use Committees at The University of Chicago accredited by the Association for Assessment and Accreditation of Laboratory Animal Care (AAALAC).

Germ free mice

Germ-free (GF) BALB/cJ, I/LnJ, C3H/HeN, BALB/cJ-H-2^J, I/LnJ-H-2^K were re-derived at Taconic Biosciences through an embryo transfer procedure. GF C57BL/6J (B6) mice were a gift from Dr. E. Chang (The University of Chicago).

Eight-week-old males and females were used at approximately 50:50 ratio in all experiments.

METHOD DETAILS

Monitoring sterility in gnotobiotic isolators

DNA was extracted from freshly frozen caecal contents or fecal pellets using a bead-beating/phenol–chloroform extraction protocol (Ley et al., 2005) and amplified with a set of primers that hybridize to all bacterial 16S rRNA gene sequences (Turner et al., 1999). Tests were conducted weekly using fecal samples from individual cages. Additionally, microbiological cultures were set up with GF fecal pellets, positive (SPF mouse fecal pellets), sham (sterile saline), and negative (sterile culture medium) controls for each sample batch. Samples were inoculated into BHI, Nutrient, and Sabaroud Broth tubes. Every sample in each of the respective culture media was incubated at 37°C and 42°C in both aerobic and anaerobic environments. Cultures were monitored daily for evidence of growth and were followed for 5 days until cultures were declared negative.

Transfer of gastrointestinal microbiota

SPF B6NTac donors of the commensal microbiota were housed in gnotobiotic isolators for a week upon arrival to recover from transportation-induced stress. SPF C57BL6/J mice were used straight from the shelf in our animal room. Donors were euthanized and their cecal contents were immediately homogenized in sterile PBS and gavaged (0.4 mL/mouse) into recipient germ free mice of both genders (generation 0, G0), which were then bred. Cecal microbiota of their progeny [generation 1 (G1)] was analyzed at 8 weeks of age.

DNA extraction, 16S rRNA amplicon sequencing and analysis

Cecal contents and IgA-coated and non-coated bacterial fractions were collected and snap frozen at –80°C. DNA was extracted from the samples using the DNeasy PowerSoil HTP 96 Kit (QIAGEN, Germantown, MD) according to the manufacturer's instructions. The V4 region of the 16S rRNA-encoding gene (515F-806R) was PCR amplified to survey the total bacterial community in the extracted samples using the Illumina MiSeq platform as described (Walters et al., 2015; Caporaso et al., 2012). PCR reactions were carried out in triplicate for each sample using sterile, DNase-free 96 well plates with appropriate (DNA template-free) negative controls using the 5 PRIME HotMasterMix kit (Quantabio, Beverly, MA). PCR reactions were conducted using an initial denaturation step of 95°C for 3 min, followed by 35 cycles at 95°C for 30 s, 55°C for 45 s, then 72°C for 1.5 min. A single extension step at 72°C for 10 min was used at the end. Triplicate PCR reactions were then pooled together, primer dimers were removed from the pooled products using the UltraClean 96 PCR Cleanup Kit (QIAGEN, Germantown, MD) and total DNA was quantified using the PicoGreen® dsDNA Assay (Invitrogen/Thermo Fisher Scientific, Carlsbad, CA) and resuspended at 2 ng/μl. Amplicons were sequenced on an Illumina MiSeq using 151 × 151 base pair paired-end sequencing at the Environmental Sample Preparation and Sequencing Facility at Argonne National Laboratory. Raw sequence data were processed using the QIIME 1.9 analysis pipeline (Caporaso et al., 2010b). Initially, paired-end reads were joined and then aligned to a database of reference sequences using PyNAST (Caporaso et al., 2010a). These were clustered into operational taxonomic units (OTUs) using UCLUST at 97% similarity (Edgar, 2010), and a consensus taxonomy from the Greengenes reference database (McDonald et al., 2012) was assigned to each sequence using the UCLUST taxonomy assigner. The accession number for 16S sequencing data reported in this paper is Github:<https://github.com/akds/microbiome-MHC>.

RNA isolation, sequencing (RNASeq), and analysis

Duodenum, jejunum, ileum, and colonic sections were harvested and washed with two volumes of 10 mL each of PBS to clear luminal contents. Immediately following collection, samples were stored at –80°C. RNA from intestinal tissues was isolated using a PureLink RNA Mini Kit (Thermo Fisher Scientific). All samples were DNase treated during RNA purification.

RNASeq libraries were prepared using Illumina TotalRNA TruSeq kits (RiboZero depletion) and sequenced using an Illumina HiSeq4000 (single-end 50bp).

Sequence identity of genes expressed differentially between BALB/cJ and C57BL/6J mice was determined using a BLASTN alignment of the reference C57BL/6J transcript to the BALB/cJ genome (http://useast.ensembl.org/Mus_musculus_BALB_cJ/Info/Index; default settings). Multiple putative alignments were distinguished based on the longest full-length alignment of the reference transcript to the BALB/cJ genome. The percentage of the aligned transcript sequence that is identical to the BALB/cJ genome sequence was calculated. The median sequence BLAST identity from one or more exons of the transcript was reported. The accession number for RNA-seq data reported in this paper is GEO:GSE136572.

Purification of IgA-coated and uncoated bacteria from colons

Colonic contents stored at –80°C were resuspended in sterile PBS and protease inhibitor (Roche) at 10mg of cecal contents per 100 μL of PBS. Mixtures were vortexed and centrifuged at 400 g to pellet debris. The supernatant was filtered through 70 μm nylon mesh and centrifuged at 8000 g for 5 min. The bacterial pellet was resuspended in sterile PBS/0.25% BSA/10% normal goat serum (Jackson ImmunoResearch) and stained with goat anti-mouse IgA antibodies (Southern Biotech). IgA-positive and IgA-negative fractions were isolated by autoMACS (Miltenyi). The bacterial pellet was resuspended in 5μM SYTO-13 (Life Technologies), and then stained with anti-mouse IgA-biotin (Southern Biotech), followed by streptavidin-APC (BioLegend). SYTO-13-positive, APC-negative or positive populations were sorted using a BD FACS Aria III.

Real-time quantitative PCR

An Applied Biosystems StepOnePlus Real-Time PCR system and SYBR Green master mix (Thermo Fisher Scientific) were used to perform real-time PCR on cecal DNA isolated from recipient gnotobiotic BALB/cJ, BALB/cJ RAG1^{-/-}, BALB.B, C57BL/6J mice and donor B6NTac mice. Each reaction was performed in technical triplicates. Primers specific to mouse SFB (SFB736F- GACGCT GAGGCATGAGAGCAT, SFB844R- GACGGCACGGATTGTTATTCA (Barman et al., 2008) and broad-range 16S rRNA primers (Uni 926F- AAACCTCAAAGGAATTGACGG, Uni 1062R- CTCACRRCACGAGCTGAC) (Bacchetti De Gregoris et al., 2011) were used. The $2^{-\Delta\Delta CT}$ log₂ (fold change) was calculated as follows: $\Delta CT = CT$ for an individual DNA sample amplified with SFB specific primers minus CT for the same sample amplified with broad range 16S rRNA primers; $\Delta\Delta CT = \Delta CT$ minus average CT for all B6 DNA samples amplified with 16S ribosomal RNA specific primers. Graphs and statistics were generated using Prism 8 (GraphPad).

QUANTIFICATION AND STATISTICAL ANALYSIS

Statistical analysis of the 16S dataset was carried out with the MATLAB (MathWorks, Natick, MA, USA) software package. Principal component analysis (PCA) of the microbiomes was performed using the relative abundance of genera from each sample. The percent variance explained by each principal component was calculated and reported in corresponding figures. Principal coordinate analysis (PCoA) visualization was also generated using multidimensional scaling with Bray–Curtis metric and Weighted UniFrac as distance measures. To establish if there was a significant difference between two conditions, the β diversity of samples in a specific comparison was estimated using the Bray–Curtis distance. A one-sided non-parametric Wilcoxon rank sum test was then used to determine if the microbial differences between strains (or distances of all pairs of mice between two conditions) was greater than differences within a strain.

Differentially abundant OTUs between conditions were identified using an unpaired two-sample t test. We controlled for multiple-hypothesis testing with the q value method by adjusting the p value to reflect the false discovery rate using the procedure described by Storey (2002). Significantly different OTUs classified at the genus level (adjusted $p < 0.05$) were depicted using a red-blue heatmap where OTU abundance was transformed with zero mean and unit variance across all mice. Nonspecific OTUs not classified at the genus level were marked with asterisks (*) and reported using the most specific higher taxonomic classification level (family, order or class) associated with the OTU. Family level OTUs were used for PCA visualization and the percent variance explained by each axis was reported.

RNA-seq reads were aligned to the *Mus musculus* reference C57BL/6J transcriptome with Ensembl gene annotation (GRCm38) by Kallisto (v0.44.0; default settings) (Bray et al., 2016) in order to generate mRNA expression quantifications. The k mer-based pseudoalignment algorithm performed by Kallisto is robust to minor differences between reads and the reference transcriptome and, thus, is reasoned to be well suited for instances of modest genetic differences between strains. mRNA expression was quantified at transcript level (transcript per million; TPM) and then summarized into gene level (TPMs summed over all gene transcripts) measurements. Gene level TPMs were log₂(n+1)-transformed for further analysis. Differentially expressed genes between BALB/cJ and C57BL/6J were identified using two criteria: (1) an unpaired two-sample t test and (2) log₂ expression difference greater > 1 . We controlled for multiple-hypothesis testing with the q value method by adjusting the p value to reflect the false discovery rate using the procedure described by Storey (2002).

All qPCR assays were done in triplicate ($n = 3$). Error bars represent standard deviation (SD). Significance for real-time PCR was calculated by ordinary one-way ANOVA.

The statistical details of experiments can be found in the figure legends, figures, and experimental procedures including the statistical tests used; exact value of n , where n represents the number of animals used in experiments, is either indicated or is obvious from the number of symbols representing individual animals; and precision measures (mean value and SD). No randomization or blinding was used.

DATA AND CODE AVAILABILITY

The datasets generated during this study are available at GEO: GSE136572 and <https://github.com/akds/microbiome-MHC>

Cell Reports, Volume 29

Supplemental Information

Polymorphic Immune Mechanisms

Regulate Commensal Repertoire

Aly A. Khan, Leonid Yurkovetskiy, Kelly O'Grady, Joseph M. Pickard, Renée de Pooter, Dionysios A. Antonopoulos, Tatyana Golovkina, and Alexander Chervonsky

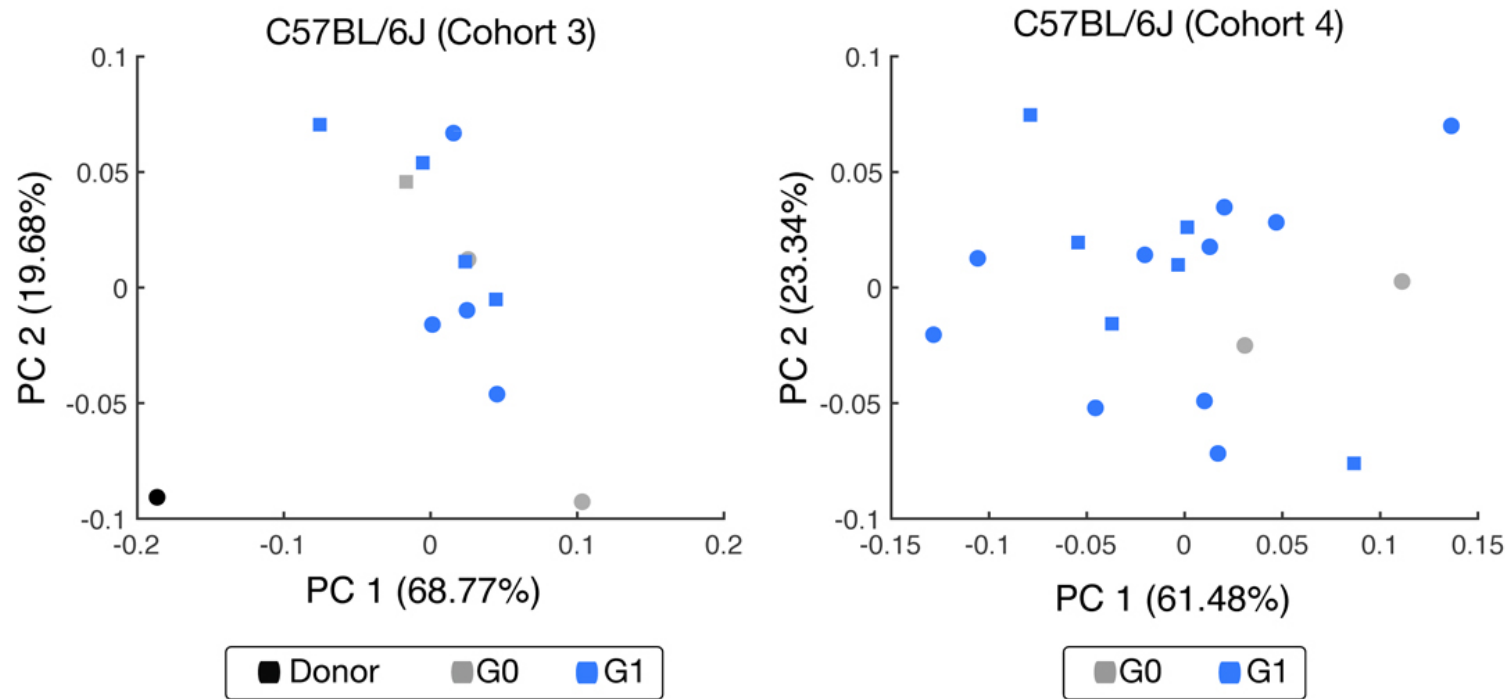


Figure S1. PCA showing that G0 microbiomes are not separable from G1 in two independent experiments. Related to Figure 1. Donor - B6 microbiota. Circles, females; squares, males.

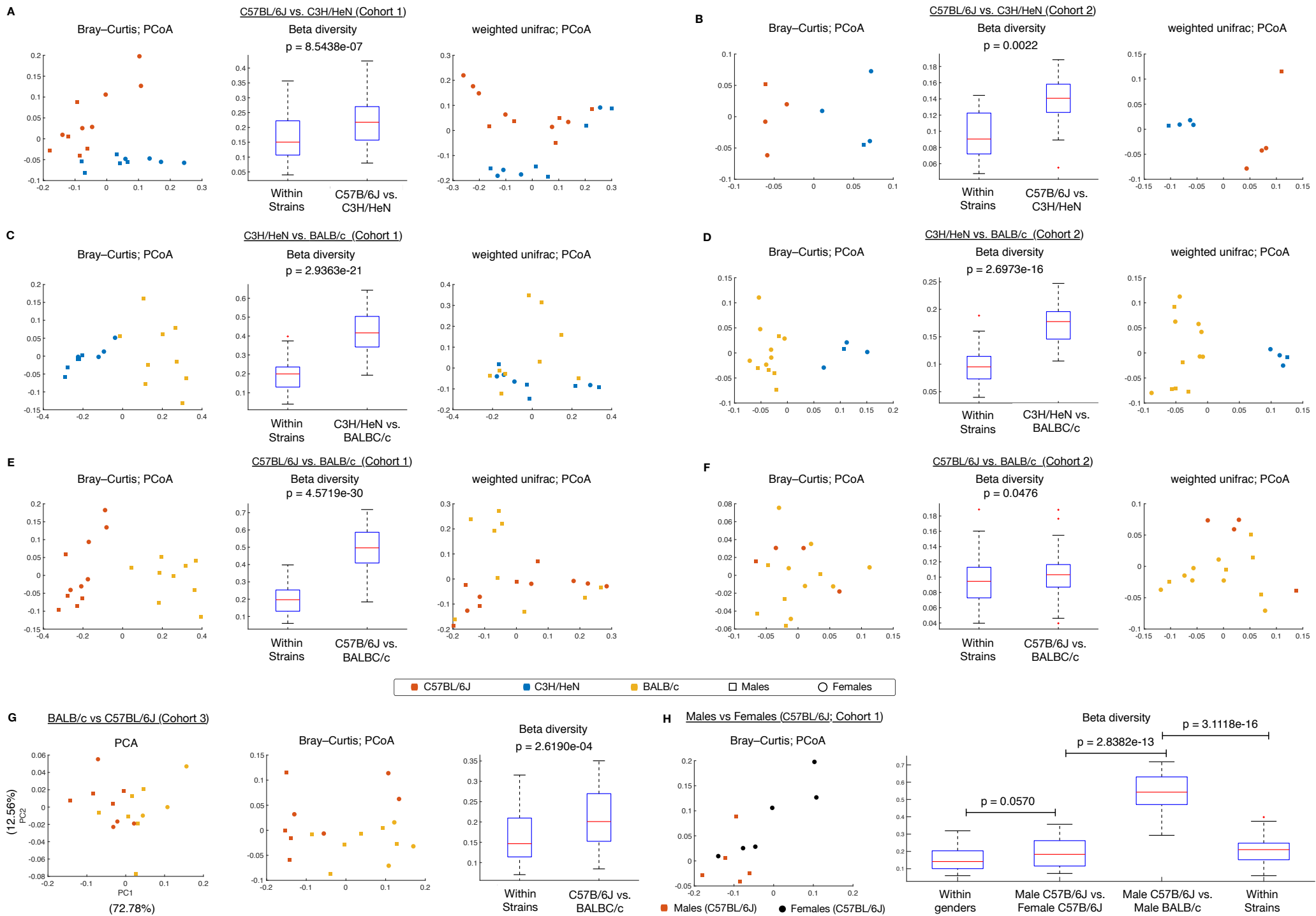


Figure S2. Principal coordinate analysis (PCoA) and comparison of β diversity between various strains colonized with C57BL/6J microbiota. Related to Figure 2.

A-F. PCoA was performed using Bray–Curtis distance (left) and Weighted UniFrac distance (right), demonstrating reproducible separation of strains using two different distance metrics; a non-phylogenetic based metric (Bray–Curtis) and a phylogenetic based metric (Weighted UniFrac).

One-sided non-parametric Wilcoxon rank sum test was used to determine if the β diversity estimated using Bray-Curtis distance metric between strains was greater than differences within a strain. The following comparisons are shown: C57BL/6J vs. C3H/HeN (Cohort 1) (**A**); C57BL/6J vs. C3H/HeN (Cohort 2)(**B**); C3H/HeN vs. BALB/c (Cohort 1) (**C**); C3H/HeN vs. BALB/c (Cohort 2) (**D**); C57BL/6J vs. BALB/c (Cohort 1) (**E**); C57BL/6J vs. BALB/c (Cohort 2) (**F**).

G. Comparison of the microbiomes of two ex-GF strains (BALB/c vs C57BL/6J) colonized with the same microbiotas from Cohort 3 shown as PCA (left), PCoA using Bray–Curtis distance (center), and β diversity estimated using Bray-Curtis distance metric between strains (right).

H. Comparison of the microbiomes of male and female ex-GF C57BL/6J mice from Cohort 1 shown as PCoA using Bray–Curtis distance. Males are represented by red rectangles, females by black circles (left). One-sided non-parametric Wilcoxon rank sum tests were used to examine if strain differences are greater than gender differences (right). β diversity found between male C57B/6J and female C57B/6J mice showed a strong trend for being greater than β diversity found within gender among C57B/6J mice ($p = 0.0570$). The β diversity found between male C57B/6J and male BALB/c mice was significantly greater than β diversity found between male C57B/6J and female C57B/6J ($p = 2.8382e-13$). The β diversity found between male C57B/6J and male BALB/c mice is significantly greater than β diversity found among male mice within strains ($p = 3.1118e-16$).

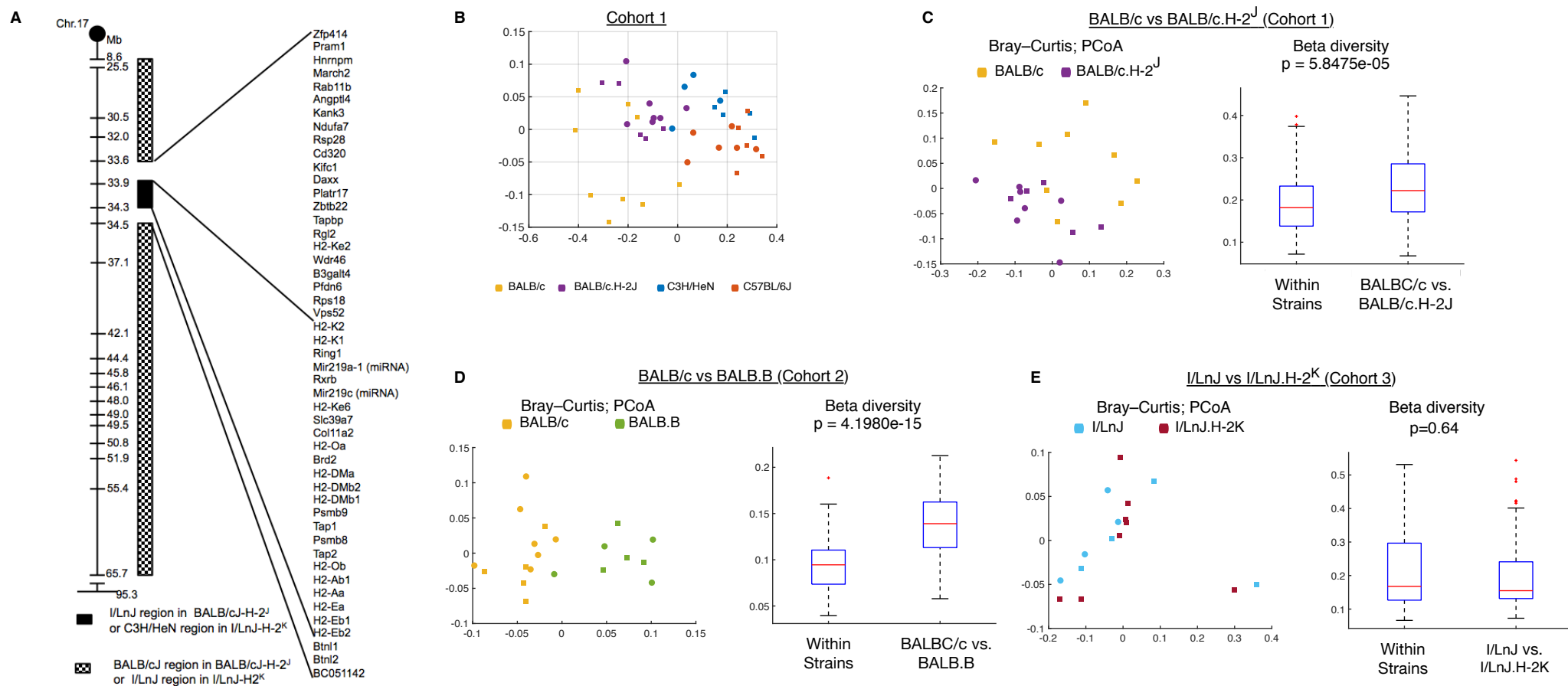


Figure S3. Additional analyses of microbiomes of MHC-congenic strains of mice. Related to Figure 3.

A. Schematic map of the congenic BALB/cJ line containing the MHC locus from I/LnJ mice and I/LnJ mice containing the MHC locus from C3H/HeN mice. The replacement was achieved by crossing the two strains followed by multiple back-crossings to BALB/cJ mice and I/LnJ mice respectively. At generation N10 mice in both back-crosses were intercrossed. Open areas upstream and downstream of the MHC locus - regions of undefined origin.

B. 2-D PCA analysis of the microbiomes of BALB/cJ (yellow), BALB/c-H-2j (magenta), C3H/HeN (blue) and C57BL/6J (red) mice. Dots – females, squares – males. 3-D plot of the same data analysis is shown in Figure 3A.

C-E. Principal coordinate analysis (PCoA) visualizations and comparison of β diversity between various strains colonized with C57BL/6J microbiota. PCoA performed using Bray-Curtis distance (left) and one-sided non-parametric Wilcoxon rank sum tests used to examine if strain differences are greater than gender differences (right): BALB/c vs BALB/c.H-2J (Cohort 1) (**C**); BALB/c vs BALB.B (Cohort 2) (**D**); I/LnJ vs I/LnJ.H-2K (Cohort 3) (**E**).

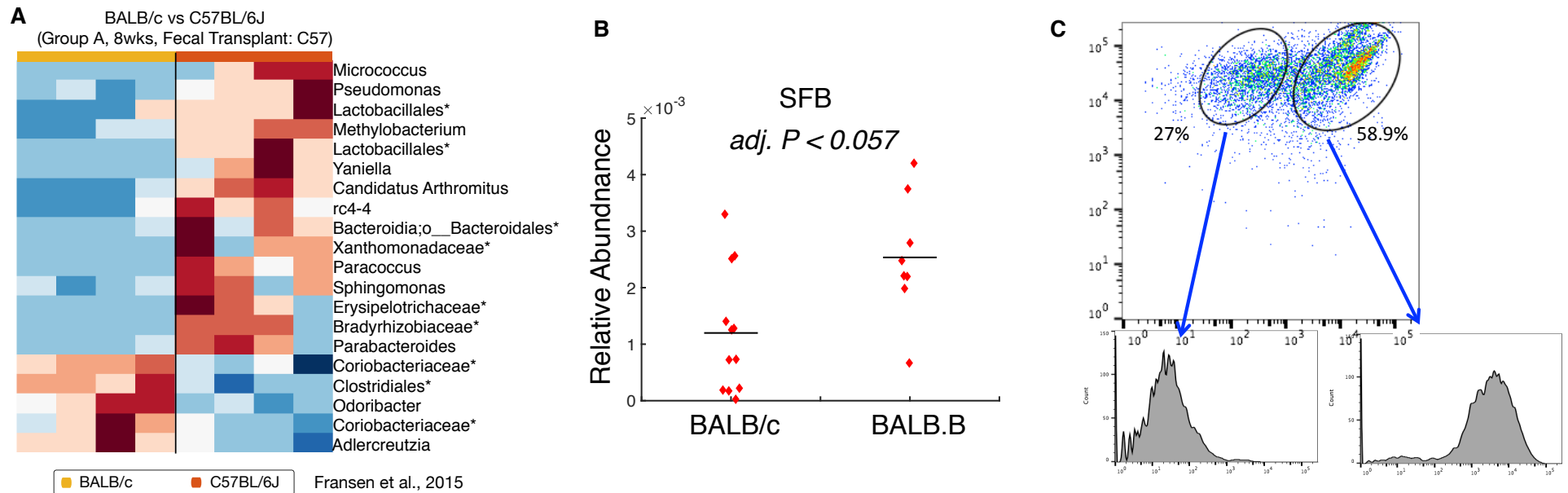


Figure S4. Additional analyses of the microbiomes. Related to Figure 3

A. Data from Fransen et al., 2015 reanalyzed. Heat map showing statistically significant lineage differences ($P < .05$, FDR adjusted t-test) of bacterial lineages between ex-GF BALB/c vs. C57BL/6J 8 weeks after fecal transplant with B6 microbiota. Notably, *Candidatus Arthromitus* (SFB) was higher in C57BL/6J.

B. Relative abundance of SFB bacteria in BALB/cJ (H-2^d) and BALB.B (H-2^b) mice from our high throughput sequencing experiment (Cohort 3).

C. An example of sorting of colonic bacteria for IgA-seq experiments. Colonic contents free of debris was stained with anti-IgA antibodies conjugated to the APC fluorochrome and sorted into + and - populations, which were reanalyzed before extracting DNA for sequencing.

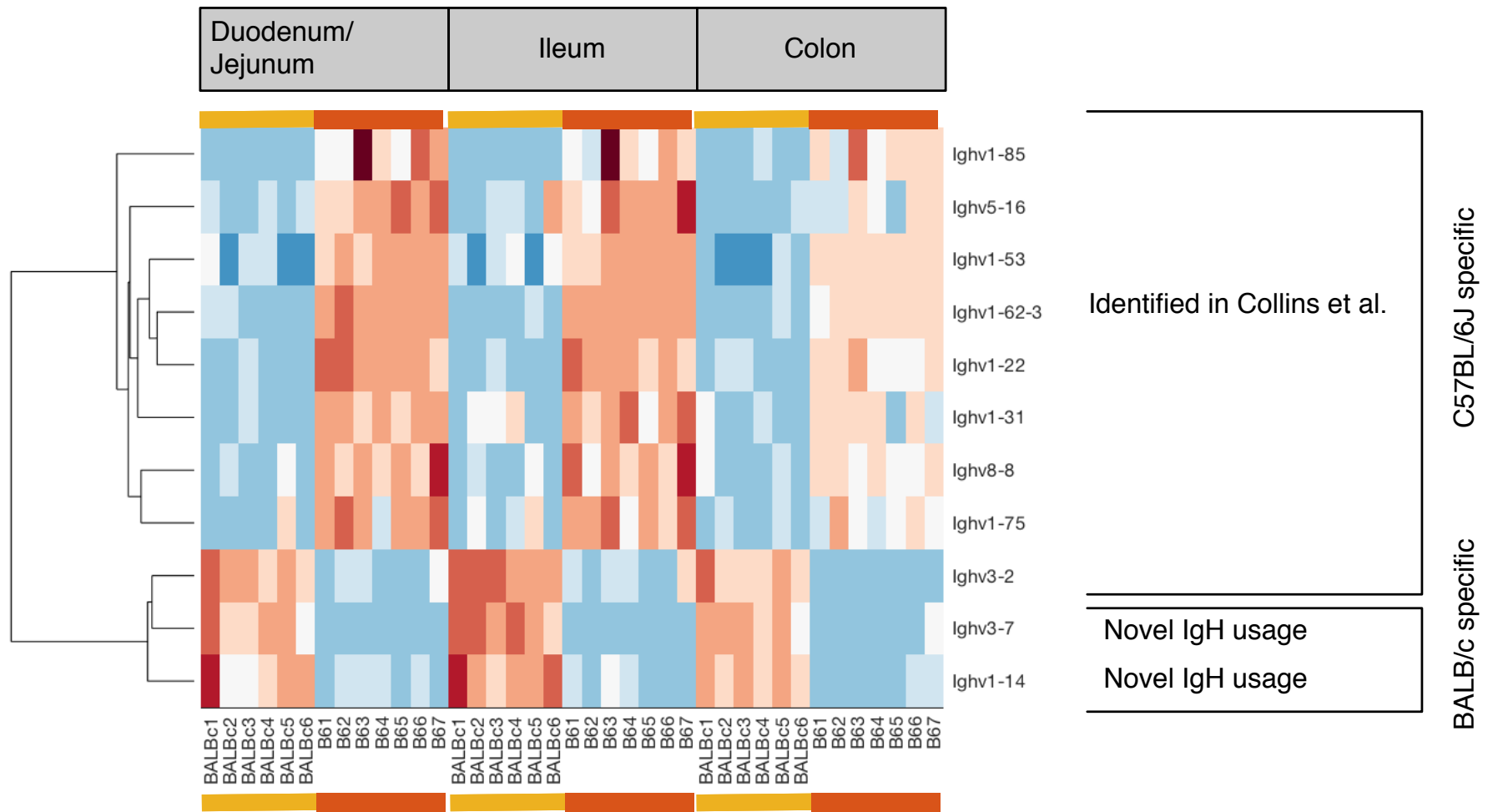


Figure S5. BALB/cJ and C57BL/6J mice utilize different families of the variable regions of the heavy chain of immunoglobulins. Related to Figure 4. Some of these differences were reported before (Collins et al, 2015), some are reported here.

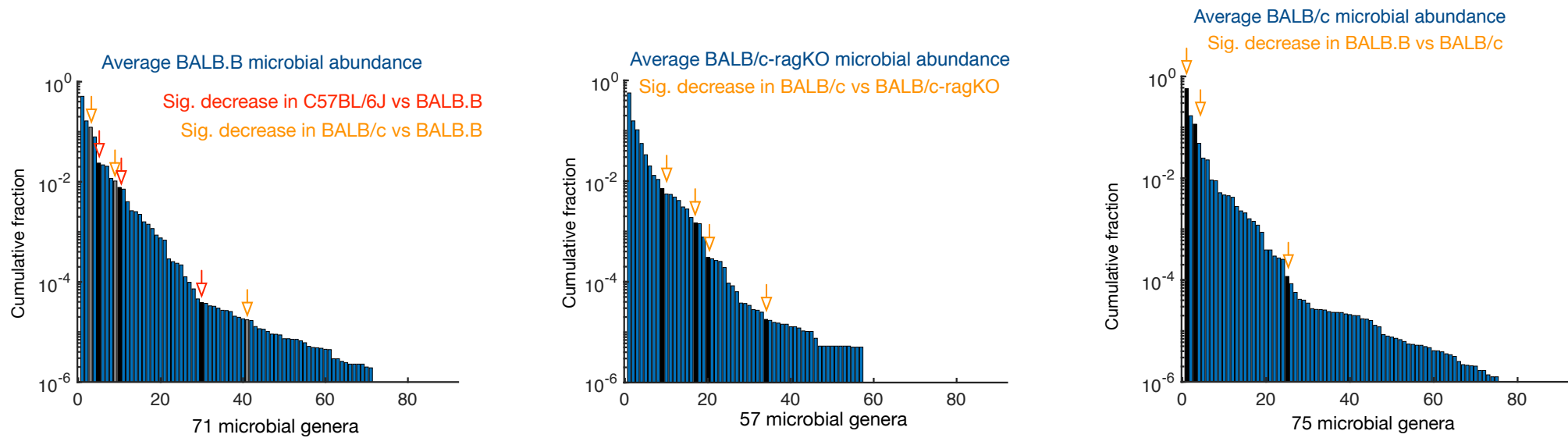


Figure S6. Limited number of bacterial lineages is controlled by polymorphic innate and adaptive mechanisms. Related to Figure 3. Arrows show abundances of bacterial lineages significantly different between indicated strains of mice. Abundance itself was not a factor for controlling mechanisms – lineages with higher and very low abundances were selectively controlled.

Table S1. Input microbiota, cohort structure and mouse numbers in the current study. Related to Figures 1-4.

Cohort	Source of microbiota	G0 strains	G1		Total number of mice per group per experiment	
			F	M		
1	B6 UC (JAX)	B6	1F	2	1	11
		B6	1F	4	4	
		BALB/cJ	1F	0	10	10
		BALB.H-2 ^l	1F	7	5	12
		C3H/HeN	1F	4	5	9
2	B6 TAC	BALB/cJ Rag1 ^{-/-}	1F	1	2	5
		BALB/cJ Rag1 ^{-/-}	1F	1	1	
		C57BL/6J	1F	1	1	4
		C57BL/6J	1F	2	0	
		BALB.H-2 ^l	1F	0	4	7
		BALB.H-2 ^l	1F	3	0	
		BALB/cJ	1F	2	3	12
		BALB/cJ	1F	5	2	
		I/LnJ	1F	1	2	12
		I/LnJ	1F	1	4	
		I/LnJ	1F	2	2	
		C3H/HeN	1F	1	1	4
		C3H/HeN	1F	2	0	
		BALB.H-2 ^b	1F	2	2	8
		BALB.H-2 ^b	1F	2	2	
3	B6 TAC	I/LnJ.H-2 ^k	1F	0	4	8
		I/LnJ.H-2 ^k	1F	0	4	
		BALB/cJ	1F	2	4	10

		BALB/cJ	1F	1	3	
		I/LnJ	1F	2	3	8
		I/LnJ	1F	2	1	
		B6	1F	2	2	8
		B6	1F	2	2	
4	B6 JAX	B6	1F	3	2	16
		B6	1F	2	2	
		B6	1F	5	2	

Sources of microbiota for GF mice repopulation: Cohort 1 - B6 (UC) JAX originated from The Jackson Laboratory, but were bred and housed at the University of Chicago for several generations; Cohorts 2 and 3 – donors arrived straight from Taconic; B6 JAX – donors arrived straight from The Jackson Laboratory.

Each line shows the size and gender break of the progeny of a particular G0 female.

Last column summarizes mouse numbers used for statistical analysis in each experiment (cohort).

Table S2. Selected genes with differential expression in BALB/c and B6 gut chosen by relevant gene ontology (GO) category and relevance to immunity and/or inflammatory conditions in the gut. Related to Figure 4.

Physiological function Gene name	GO ID	GO process association	Association with immunity and disease	References
Complement activation <i>C1rb</i> <i>C1s2</i>	0006956 0006956	Complement activation Complement activation		
Mucosal pentraxins <i>Mptx1</i> <i>Mptx2</i>			Microbial dysbiosis Antimicrobial peptide expressing Paneth cells	(van der Meer- van Kraaij et al., 2007) (Haber et al., 2017)
Inactivators of xenobiotics and toxins <i>Ces1b</i> <i>Fmo4</i> <i>Gsta1</i>	0016042 0055114 0006749	Lipid catabolic process TMAO inactivation Glutathione metabolism	Enzymatic hydrolysis Gut microbiota cardio-vascular disease	(Hosokawa, 2008) (Wang et al., 2011)
NK cell differentiation and activation <i>H60c</i> <i>Il11ra2</i> <i>Raet1e</i>	0001913 0004896 0001913	Cell mediated cytotoxicity Cytokine receptor activity Cell mediated cytotoxicity		
Glycosyltransferases <i>St3gal4</i>	0006486	Protein glycosylation	Intestinal inflammation and microbial dysbiosis	(Huang et al., 2015)
Trim proteins – regulators of inflammation and anti-viral immunity <i>Trim30d</i> <i>Trim34b</i> <i>Trim80</i>			Innate immunity and pathogen recognition	(Ozato et al., 2008) (Ozato et al., 2008) (Ozato et al., 2008)
Gasdermins <i>Gsdmc3</i> <i>Gsdms4</i>	0012501 0012501	Programmed cell death Programmed cell death	Inflammatory bowel disease Inflammatory bowel disease	(Yuan et al., 2018) (Yuan et al., 2018)

Reactive oxygen species production/Oxidation of microbial metabolites <i>Duox1</i>	0019221	Cytokine-mediated signaling pathway	Gastric colonization by <i>H. Felis</i>	(Grasberger et al., 2013)
Neutrophil function <i>Prg2</i> <i>Padi4</i> <i>Tmem116</i>	0002376 0002376	Immune system process Immune system process	Crohn's disease Septic shock mortality	(Han et al., 2013) (Costa et al., 2018)
Intestinal barrier function <i>Afm</i> <i>Tjap1</i> <i>Pianp</i>	0008431 0005923 0050776	Vitamin E binding Bicellular tight junction	Intestinal homeostasis	(Mihara et al., 2016)
Peptidase inhibitors <i>Serpina10</i> <i>Serpina1a</i> <i>Serpina1b</i> <i>Serpina3a</i> <i>Serpina3h</i>	0010466 0010466 0010466	Negative regulation of peptidase activity Negative regulation of peptidase activity Negative regulation of peptidase activity		
Interferon-induced genes <i>Iff44l</i> <i>Iff202b</i> <i>Gvin1</i>	0006955 0045087	Immune response Innate immune response	Microbial diversity correlated with expression of these genes Immunity to intracellular pathogens	(Brodziak et al., 2013) (MacMicking, 2004)
Inflammasome regulation <i>Nlrp1b</i>	0045087	Innate immune response	Colitis	(Williams et al., 2015)
Macrophage phagocytic function <i>Spp1</i>	0006954	Inflammatory response		(Toyonaga et al., 2015)
Metabolic genes <i>Eno1b</i> (retrotransposed)			<i>H. Pylori</i> -mediated gastric diseases	(Chen et al., 2014)

Table S3. Complete list of genes with significant difference in expression between BALB/c and B6 gut. Related to Fig.4. Variable regions of immunoglobulin genes are shown separately. DJ-duodenum/jejunum.

Duodenum/Jejunum	Host Genes		Immunoglobulin Genes		
	Ileum	Colon	IG-DJ	IG-Ileum	IG-Colon
1700011H14Rik	1700011H14Rik	2010005H15Rik	Ighv1-14	Ighv1-13	Ighv1-14
2200002J24Rik	2200002J24Rik	5830417110Rik	Ighv1-15	Ighv1-14	Ighv1-15
5830417110Rik	5830417110Rik	9530053A07Rik	Ighv1-22	Ighv1-15	Ighv1-2
9530053A07Rik	9530053A07Rik	Actc1	Ighv1-31	Ighv1-22	Ighv1-20
Acta1	A930018M24Rik	Afm	Ighv1-39	Ighv1-23	Ighv1-22
Actc1	Acta1	AK157302	Ighv1-53	Ighv1-27	Ighv1-23
AK157302	Actc1	Apoa2	Ighv1-56	Ighv1-31	Ighv1-25
BC035947	AK157302	Atp8b5	Ighv1-58	Ighv1-36	Ighv1-27
Camk2b	Akt2-ps	BC025446	Ighv1-62	Ighv1-38	Ighv1-30
Clec2j	Apoa2	C1rb	Ighv1-62-2	Ighv1-43	Ighv1-31
Cyp2c29	BC035947	C1s2	Ighv1-62-3	Ighv1-53	Ighv1-33
Cyp2c67	C1rb	Cib3	Ighv1-71	Ighv1-58	Ighv1-36
Cyp3a59	C1s2	Col4a6	Ighv1-75	Ighv1-62	Ighv1-37
Defa-ps18	Ces1b	Cyp2c67	Ighv1-76	Ighv1-62-2	Ighv1-43
Defa2	Clec2j	Cyp2r1	Ighv1-78	Ighv1-62-3	Ighv1-53
Defa20	Col4a6	Dynlt1a	Ighv1-81	Ighv1-71	Ighv1-62-3
Defa21	Cyp2c67	Ear-ps3	Ighv1-84	Ighv1-75	Ighv1-67
Defa22	Cyp3a44	Eno1b	Ighv1-85	Ighv1-84	Ighv1-75
Defa26	Defa-ps18	ENSMUST00000012440.12	Ighv10-3	Ighv1-85	Ighv1-81
Defa27	Defa-ps5	ENSMUST000000160663.1	Ighv14-4	Ighv1-86	Ighv1-83
Defa28	Defa-ps8	Fmo4	Ighv2-9	Ighv2-9	Ighv1-85
Defa32	Defa2	Gbp10	Ighv3-1	Ighv3-1	Ighv1-86
Defa33	Defa20	Gbp2b	Ighv3-2	Ighv3-2	Ighv14-4
Defa35	Defa21	Gvin1	Ighv3-7	Ighv3-7	Ighv2-4
Dynlt1a	Defa22	H2-Ea-ps	Ighv5-16	Ighv4-2	Ighv2-6
Eno1b	Defa26	H2-Q3	Ighv7-2	Ighv5-16	Ighv2-6-8
ENSMUST000000116					
434.9	Defa27	H60c	Ighv8-8	Ighv7-2	Ighv2-9
Gsdmc3	Defa28	Hist1h2aa	Igkv1-99	Ighv8-11	Ighv3-1
Gsdmc4	Defa32	Hist1h2ao	Igkv4-62	Ighv8-8	Ighv3-2
Gvin1	Defa33	Hmga1-rs1		Igkv7-33	Ighv3-7
H2-Ea-ps	Duox1	I830127L07Rik		Igkv8-31	Ighv4-2
H2-K2	Dynlt1a	Ifi202b			Ighv5-16
Hist1h2aa	Eno1b	Ifi44l			Ighv5-2
	ENSMUST00000001				
Hist3h2bb-ps	2440.12	Ii11ra2			Ighv6-6
	ENSMUST00000009				
Hmga1-rs1	0860.6	Klk15			Ighv6-7
Hmgb1-ps8	Gsdmc4	Lrmda			Ighv7-2
Ifi202b	Gsdmcl2	Marcksl1-ps4			Ighv7-4
Ifi44l	Gsta1	Mptx2			Ighv8-11
Itpa-ps1	Gvin1	Mrpl48-ps			Ighv8-2
Mcoln3	H2-Ea-ps	Mrto4-ps2			Ighv8-8

Mptx1	H2-Q3	Mup-ps23	Igkv1-88
Mrpl48-ps	Hist1h2aa	Nlrp1b	Igkv3-2
Msantd1	Hist1h2ao	Nxpe4	Igkv4-50
Nlrp1b	Hist2h2aa2	Nxpe5	Igkv4-79
Nlrp1c-ps	Hmga1-rs1	Oas2	Igkv4-92
Pnp2	Hmgb1-ps8	Padi4	Igkv7-33
Prg2	I830127L07Rik	Pkhd1	
Rbpsuh-rs3	Ifi202b	Pnp2	
Rpl15-ps1	Ifi44l	Raet1e	
Rpl3-ps1	Il11ra2	Rbpsuh-rs3	
Rplp0-ps1	Insl3	Rpl3-ps1	
Rps12-ps9	Mptx1	Rpl35a-ps2	
Rps3a2	Mrpl48-ps	Rpl35a-ps3	
Serpina3a	Nlrp1b	Rpl35a-ps4	
Skiv2l-ps1	Nlrp1c-ps	Rpl35a-ps6	
Sprr2a1	Nr0b2	Rpl36-ps2	
Sspo	Nudc-ps1	Rplp0-ps1	
St3gal4	Pianp	Rps12-ps9	
Sycp1	Pik3c2g	Rps3a2	
Tdg-ps	Pnp2	Serpina1a	
Them7	Rbpsuh-rs3	Serpina1b	
Tjap1	Rpl3-ps1	Skiv2l-ps1	
Tmem116	Rpl35a-ps2	Slc22a29	
Tpm3-rs7	Rpl35a-ps3	Sycp1	
Trbv29	Rpl35a-ps4	Tdg-ps	
Trim34b	Rpl35a-ps6	Tdpx-ps1	
Trim80	Rplp0-ps1	Tpm3-rs7	
Vmn1r212	Rps12-ps9	Trim30c	
Wsb2-ps	Rps2-ps6	Trim30d	
	Rps3a2	Trim34b	
	Serpina10	Unc5a	
	Serpina3h	Wsb2-ps	
	Sh2d6		
	Sh2d7		
	Skiv2l-ps1		
	Spp1		
	Sprr2a1		
	Sspo		
	St3gal4		
	Sycp1		
	Tdg-ps		
	Tdpx-ps1		
	Them7		
	Tjap1		
	Tmem116		
	Tpm3-rs7		
	Trbv29		

Trim34b

Trim80

Wsb2-ps